Princeton Plasma Physics Laboratory

PPPL-5194

Blob Structure and Motion in the Edge of NSTX

S.J. Zweben[1], J.R. Myra[2], W.M. Davis[1], D.A. D'Ippolito[2], T.K. Gray[3], S.M. Kaye[1], B.P. LeBlanc[1], R.J. Maqueda[1a], D.A. Russell[2], D.P. Stotler[1] and the NSTX-U Team

[1] Princeton Plasma Physics Laboratory, Princeton NJ 08540 USA

[2] Lodestar Research Corporation, Boulder, CO 80301, USA

[3] Oak Ridge National Laboratory, Oak Ridge TN 37831, USA

[a] Presently at: X Science LLC, Plainsboro, NJ 08536 USA

September 2015

PPPL PRINCETON PLASMA PHYSICS LABORATORY

Prepared for the U.S. Department of Energy under Contract DE-AC02-09CH11466.

Princeton Plasma Physics Laboratory
Report Disclaimers

Full Legal Disclaimer

Trademark Disclaimer

PPPL Report Availability

Princeton Plasma Physics Laboratory:

http://www.pppl.gov/techreports.cfm

Office of Scientific and Technical Information (OSTI):

http://www.osti.gov/scitech/

Related Links:

U.S. Department of Energy

U.S. Department of Energy Office of Science

U.S. Department of Energy Office of Fusion Energy Sciences

Blob Structure and Motion in the Edge of NSTX

S.J. Zweben[1], J.R. Myra[2], W.M. Davis[1], D.A. D'Ippolito[2], T.K. Gray[3], S.M. Kaye[1], B.P. LeBlanc[1], R.J. Maqueda[1a], D.A. Russell[2], D.P. Stotler[1] and the NSTX-U Team

[1] Princeton Plasma Physics Laboratory, Princeton NJ 08540 USA
[2] Lodestar Research Corporation, Boulder, CO 80301, USA
[3] Oak Ridge National Laboratory, Oak Ridge TN 37831, USA

[a] Presently at: X Science LLC, Plainsboro, NJ 08536 USA

Abstract

The structure and motion of discrete plasma blobs (a.k.a. filaments) in the edge and scrape-off layer (SOL) of NSTX is studied for representative Ohmic and H-mode discharges. Individual blobs were tracked in the 2-D radial vs. poloidal plane using data from the gas puff imaging (GPI) diagnostic taken at 400,000 frames/sec. A database of blob amplitude, size, ellipticity, tilt, and velocity was obtained for ~45,000 individual blobs. Empirical relationships between various properties are described, e.g. blob speed vs. amplitude and blob tilt vs. ellipticity. The blob velocities are also compared with analytic models.

1. Introduction

The goal of this paper is to describe the structure and motion of the plasma blobs in the edge and scrape-off-layer (SOL) of the NSTX spherical tokamak. Plasma "blobs" are relatively isolated structures which are formed in the plasma edge and move radially into the SOL (sometimes called "filaments", "bursts", or "intermittent plasma objects"). The present measurements were made using a 2-D gas puff imaging (GPI) diagnostic, and compared with analytic models for blob velocity. For the sake of simplicity and clarity we focus on two specific plasma conditions: one Ohmic and one H-mode, using GPI data from 7 nearly-identical shots in each case. These results are relevant for understanding the cross-field transport in the scrape-off layer (SOL) of tokamaks, and for future comparisons of edge turbulence measurements with modeling of the SOL, e.g. for ITER.

The central concept of the outward convective motion of an isolated blob in the SOL of a tokamak was proposed by Krasheninnikov in 2001 [1], and since then there have been many refinements of the analytic theory of blob structure and motion, as described in the review papers [2,3]. Recent computational studies of blobs have shown that the expected structure and motion of blobs can become quite complicated, depending on the details of tokamak geometry [4,5], the regime of collisionality [2,3,6,7], inclusion of ion temperature effects [8-10], drift wave and other 3D effects [11-13], kinetic effects [14-16], and density gradients [17-18] Even the relationship between simplified analytic blob models and the results of computational simulations is not always clear, since the analytic models generally do not describe the blob formation process or blob-blob interactions. Some recent models describe blobs only in a statistical sense [19-21].

Given the complexity of blob theory and the difficulty of blob measurements in tokamaks, it is not surprising that the connection between blob experiments and theory is imprecise and incomplete. A review in 2011 [3] plotted the dimensionless blob sizes and radially velocities for nine tokamaks vs. two analytic blob models (sheath-connected and inertial regimes), and showed that most of the data points fell between these two scalings,

but with considerable uncertainty and scatter. More recently, agreement of radial blob velocities at about the 50% level with a warm ion model could be obtained for selected discharges on ASDEX-Upgrade [22]. In a different set of experiments, a regime transition for blob dynamics was correlated with collisionality in the MAST divertor [5], and clearer comparisons have been obtained for blobs in simpler magnetic geometries, such as Torpex [23] and VTF [24].

The present paper builds on several previous experimental and theoretical studies of blobs in NSTX. The initial GPI results using HeI line emission showed a broad spread of blob velocity in both radial and poloidal directions, with a radial velocity roughly independent of blob amplitude [25]. An early theoretical comparison [26] focused on a small set of blobs in L-mode and H-mode shots, and showed that their radial motion was bounded by the minimum and maximum speeds predicted from analytic blob models. Subsequently, a reduced 2-D edge turbulence simulation was made using the SOLT code [27], and initial results were compared with fluctuation levels, blob structure, and heat flux SOL width measurements. A synthetic GPI diagnostic was added to SOLT [28] and further comparisons with GPI were made, including a sensitivity study with respect to various theoretical assumptions. Intermittent blob-filaments were observed using LiI light emission near the lower divertor plates in NSTX [29], and were highly correlated with midplane blobs measured by GPI. The intermittency in the SOL during H-modes was studied at power levels from P_{NBI} = 0-6 MW, showing the lowest blob activity in Ohmic H-modes and low blob activity shortly after L-H transitions [30]. Recent SOLT simulations and GPI data were compared with respect to the effect of edge sheared flows on blobs, and detailed GPI blob tracking for one NSTX shot was interpreted in terms of edge shear flows [31]. A set of Langmuir probe measurements in NSTX showed intermittent SOL structures with a radial size ~5-10 cm and outward velocity ~3-5 km/sec, roughly consistent with GPI measurements, along with inward propagating voids inside the separatrix [32]. Recently the variations of edge turbulence and blobs over a large NSTX GPI database was described [33]. However, that paper discussed only the average behavior of blobs in each shot (including the shots used in the present paper), but

did not describe the individual blob behavior or the statistical distribution of blobs within a given type of shot, which is the focus of the present paper.

The outline of this paper is as follows: Sec. 2 describes the plasma parameters for the shots used in this experiment, Sec. 3 describes the theoretical blob regimes, Sec. 4 describes the blob diagnostics and data analysis, and Sec. 5 gives an overall comparison of the blobs between Ohmic and H-mode regimes. Section 6 describes the blob radial velocity, Sec. 7 describes the blob poloidal velocity, and Sec. 8 describes the blob structure. Finally, Section 9 discusses blob SOL width, and Sec. 10 contains a summary and discussion.

2. Plasma parameters

Table 1 lists the main parameters for the Ohmic and H-mode discharges used in this paper, evaluated at the time of the GPI gas puff, based on seven nearly identical shots for each case (there were too few L-mode cases for a similar data set). All shots had the same plasma current (830 kA), but the H-mode shots had a slightly higher toroidal field than the Ohmic shots (B_t=4.9 kG vs. 3.6 kG), and the H-mode shots had 4 MW of neutral beam injection (NBI) and higher stored energy (W=220 kJ vs. 32 kJ for the Ohmic plasmas). All shots were lower-single-null shape with deuterium fueling, and without any transient events such as ELMs or large MHD during the time of interest. At the bottom of Table 1 are edge plasma parameters: the drift-wave gryroraius ρ_s, the electron-ion collision time τ_{ei}, and the electron beta β_e , along with a summary of blob statistics. A similar table was used previously in a paper describing the larger database [33].

The edge profiles of T_e and n_e from the Thomson scattering diagnostic at the time of the GPI gas puff are shown in Figs. 1(a) and 1(d), averaged over the 7 shots of each type. These data are plotted with respect to the EFIT separatrix position (which varied by less than 1 cm within each type), and show the shot-to-shot standard deviations as error bars. As expected, inside the separatrix (i.e. radius $\leq$ 0 cm) the T_e and n_e are much higher

for the H-mode plasmas, but outside the separatrix the values are more similar, although uncertainties are large, particularly for H-modes at radii ≥ 2 cm. Figures 1(b) and 1(e) shows the radial gradients dT_e/dr and dn_e/dr derived from spline fits to the T_e and n_e data, which are much larger inside the separatrix than outside, and much larger for H-mode than for Ohmic plasmas. Figures 1(c) and 1(f) shows the T_e and n_e gradient scale lengths (e.g. $T_e/(dT_e/dr)$, with error bars derived from the error bars in Fig. 1(a) and 1(d). The gradient scale lengths for H-mode plasma inside the separatrix are near or below those for Ohmic plasmas, but the uncertainties are too large beyond a radius of 2 cm outside the separatrix to give useful scale lengths.

3. Blob theory regimes

Based on the plasma parameters of Sec. 2 and the geometry of NSTX, the dimensionless blob theory parameter regimes for these discharges are shown in Fig. 2. The collision disconnection factor Λ is defined by [3]:

$$\Lambda = \frac{L_{||}\nu_{ei}}{\rho_s \Omega_e} = 2.75\times10^{14}\,\frac{L_{||}(\mathrm{cm})\,n_e(\mathrm{cm}^{-3})}{T_e^2(\mathrm{eV})} \qquad [1]$$

and the normalized blob size parameter $\Theta = \hat{\delta}^{5/2}$ where $\hat{\delta} = \delta/\delta_*$ and the characteristic blob size parameter is given by:

$$\delta_* = \frac{\rho_s^{4/5} L_{||}^{2/5}}{R^{1/5}} = 53.4\,\frac{L_{||}^{2/5} T_e^{2/5}}{B^{4/5} R^{1/5}} \qquad [2]$$

where the units in the final form of Eq. 2 are in cm, eV, and Gauss for deuterium plasmas. The main features of Fig. 2 are that all blobs are within a factor of two of the characteristic size where $\hat{\delta} = 1$. In most of the SOL, and certainly in the far SOL, blobs are in the sheath-connected (sc) regime. Near the separatrix, primarily due to higher density and longer connection lengths the blobs are marginally (H-mode) or more fully

(Ohmic) resistively disconnected from the sheaths, i.e. in the regime that is often called inertial (in).

4. Blob diagnostic and data analysis

The present NSTX GPI diagnostic is the same as described recently [33]. A fast Phantom 710 camera viewed a 30 cm poloidal by 24 cm radial region in the plane perpendicular to the local B field just above the outer midplane near the separatrix. A gas manifold was attached to the nearby wall and puffed deuterium gas into this region, and the Dα light from the neutral deuterium from this puff was viewed through a 657 nm (9 nm FWHM) optical filter at 397,660 frames/sec using an 80x64 pixel array. The integration time for each frame was 2.1 μsec, the time between frames was 2.5 μsec, and the spatial resolution of the optical system was ~0.5 cm at the GPI gas cloud.

Although the GPI data is digitized for ~80 msec per shot, the data in this paper focuses on time periods within ±5 msec of the peak GPI gas puff rate, which includes 4000 frames (i.e. 40 MB) of data per shot. During this time the GPI signal level is typically 20 times the pre-puff Dα level, yet the perturbation of the gas puff on the edge plasma and edge turbulence was previously found to be negligible [34]. Typical camera signal levels are ~500-1500 counts per pixel in the region of maximum brightness in these 12 bit camera images. As usual in these GPI analyses, no attempt is made to convert the GPI Dα data into local density or temperature fluctuations; the interpretation of the GPI signals in terms of density and temperature was discussed in [33,34].

The blob tracking analysis of this GPI data was done as follows: all frames are first normalized by a 1 msec rolling time-average of neighboring time frames, in order to identify the relative local maxima in each frame, i.e. the blobs. Such normalization is appropriate since the absolute value of the GPI signals depends on the local neutral density from the GPI gas puff, which is unrelated to the background plasma. A blob is (arbitrarily) defined as a region where the local normalized level becomes ≥1.5. The

region around each of these maxima is then fit by contours, and an ellipse is fit to the half-maximum contour level. The locations of the center of these half-maximum ellipse fits were then tracked from frame-to-frame, along with their ellipticity and tilt angle. The maximum allowed displacement of a given blob between frames was limited to 10 pixels (3.8 cm) to help distinguish different blobs, thus limiting the maximum detectable velocity to 15 km/s. All blobs were saved in the database if they met these criteria for at least 2 successive frames (5 μs), but ~91% of the blobs in Ohmic plasmas and ~96% of blobs in H-mode plasma were contained in blob trails having a lifetime of $\geq$15 μsec (6 frames). Note that by this definition a blob can be either inside or outside the separatrix, and that this method does not track negative perturbations ("holes").

Figure 3 shows examples of the blob tracking done for 1 msec of an Ohmic shot (left) and 2 msec of an H-mode shot (right). The start of each blob trail is shown by an ellipse with its initial ellipticity and tilt (but not scaled to size), and each colored trail follow a blob until its end (when it fails to meet the above criteria). The average lifetime of these blob trails within the GPI field of view is τ_{blob} ~23 μsec for the Ohmic cases and τ_{blob} ~36 μsec for the H-mode cases. The database quantities calculated for each blob for each frame are: the blob center location with respect to the separatrix at that horizontal row, the normalized blob amplitude A_{blob}, the blob ellipticity (major radius/minor radius), the tilt angle (as defined in Fig. 3), the poloidal and radial sizes of the blobs L_{pol} and L_{rad} (FWHM, as in Fig. 3), and the poloidal and radial blob velocities V_{pol} and V_{rad}. Here poloidal and radial are approximated as the vertical and horizontal directions in the GPI image frames. All quantities were evaluated within the 10 msec period near the peak GPI signal, and the blob data was combined into two separate data sets, one for the 7 Ohmic shots and one for the 7 H-mode shots.

Figure 4 shows some results from the full blob database for Ohmic and H-mode separately, where each point corresponds to a single blob in a single frame. There was no significant difference between the blob results among shots of each type. The Ohmic data set shown on the left side had ~28,800 individual blobs corresponding to ~2600 blob trails like those shown in Fig. 3(a), and the H-mode data set on the right has ~18,800

blobs with ~820 blob trails. In Figs. 4(a) and 4(b) the blob amplitudes A_{blob} are shown for Ohmic cases (blue) and H-mode cases (red) as a function of the distance from the local separatrix; in Figs. 4(c) and 4(d) are the corresponding blob V_{rad}, and in Figs. 4(e) and 4(f) are the blob $V_{pol.}$ There is a wide spread in these blob properties at each radius, but there are also some systematic variations vs. radius over a spatial scale of ~2 cm, as discussed in Sec. 5.

5. Overall Comparison of Ohmic and H-mode blobs

Figure 5 shows an overall comparison of the average blob properties between the Ohmic and H-mode plasmas in this database. The individual blob statistics such as shown in Fig. 4 have been binned into 2 cm wide radial zones centered between 2 cm inside the separatrix to 6 cm outside the separatrix. Farther inside this region the blobs are entirely within closed flux surfaces, where the simplest definition of a blob [1-3] is not applicable, and farther outside this region there are too few blobs (particularly in Ohmic plasmas), and the GPI signal levels are low. The estimated uncertainty in the radial position as calculated by the EFIT reconstruction is ±1 cm.

The number of blobs detected per frame per radial zone is clearly different between Ohmic and H-mode cases, as shown in Fig. 5(a). For Ohmic plasmas the largest number of blobs per zone is found near the separatrix and few blobs were beyond 4 cm outside the separatrix, while in H-mode there were very few blobs were inside or near the separatrix, and the number of blobs was nearly constant from 2-6 cm. On average, there was ~1 blob/frame in Ohmic plasmas and ~0.5 blob/frame in H-mode plasmas within the radial region of Fig. 5. Figure 5(b) shows the normalized blob amplitudes, which are between A_{blob}=1.5 (the minimum blob amplitude by definition) and A_{blob}=3 for both types of shots up to 2 cm outside the separatrix, but increase to above 4 at 6 cm for H-mode plasmas.

The average poloidal and radial blob velocities vs. radius are shown in Figs. 5(c) and 5(d). For both Ohmic and H-mode plasmas, the magnitude of the blob V_{pol} decreases from ~3 km/sec at 0 cm to ~0.5 km/sec at 6 cm outside the separatrix, all in the negative direction (i.e. the ion diamagnetic and ion grad-B drift direction). The poloidal blob velocity at 2 cm inside the separatrix is reversed for Ohmic plasmas, as discussed previously [33]. The average blob radial velocities V_{rad} for both Ohmic and H-mode plasmas are in the range ~0.5±0.5 km/sec and radially outward. However, there is a large spread in V_{rad}, as shown by the error bars in Fig. 5(d) and data points in Fig. 4, including some inward blob velocities (see also Sec. 6).

Figures 5(e) and 5(f) show the average blob ellipticity (major/minor axis) and tilt angle (as defined in see Fig. 3). The average ellipticities are similar for Ohmic and L-mode plasmas, except for larger ellipticity at 2 cm outside the separatrix for H-mode plasmas. The tilt angles are also similar between Ohmic and H-mode plasmas, averaging ~90º±10º in all cases, indicating poloidally-elongated blob structures. Figures 5(g) and 5(h) show the average poloidal and radial blob size scales L_{pol} and L_{rad} (FWHM), which are in the range ~2-6 cm for all radii, with an average L_{pol}/L_{rad}=1.5±0.1 for Ohmic and L_{pol}/L_{rad}=1.8±0.4 for H-mode. The blob L_{pol} and L_{rad} in H-mode decrease with increasing radius, but are nearly constant vs. radius in Ohmic plasmas.

In general, it is somewhat surprising that the average blob properties of Ohmic and H-mode plasmas in Fig. 5 are so similar, given the large difference in plasma parameters inside the separatrix. Comparisons of these blob properties with theoretical models are described in the following sections.

6. Radial blob velocity

The radial blob velocity is perhaps the most interesting blob parameter, since it determines the radial transport of blobs across the SOL. There has been a considerable effort to model this velocity theoretically [1-3]. The radial blob velocities expected in the

sheath connected (sc) and inertial range (ir) regions from analytic theory relevant to these experiments are (see Fig. 2):

$$V_{sc} = c_s\,(L_{II}/R)(\rho_s/\delta_b)^2\,\tilde{n}/n \qquad [3]$$

$$V_{ir} = c_s(\delta_b/R)^{0.5}\,(\tilde{n}/n)^{0.5} \qquad [4]$$

where c_s is the sound speed, L_{II} is the parallel connection length along B to the divertor plate (L_{II} ~500 cm), R is the plasma major radius (R=85 cm), ρ_s is the ion gyroradius evaluated at the electron temperature, δ_b is the poloidal radius of the blob (i.e. $\delta_b \sim L_{pol}/2$), and $\tilde{n}/n$ is the relative density fluctuation level in the blob. If the GPI light emission is linearly dependent on the local electron density, as expected for the SOL of NSTX, then $\tilde{n}/n = 1 - 1/A_{blob}$ (this is a better definition than $\tilde{n}/n = A_{blob}$ used in [33]). Thus the theoretical results for a blob propagating in a vacuum are recovered in the limit of a large A_{blob} when $\tilde{n}/n = 1$, and $\tilde{n}/n = 0$ when $A_{blob}=1$.

Figures 6(a) and 6(b) show the distribution of individual radial blob velocities for the SOL region from 0 to + 6 cm, binned in velocity increments of 0.1 km/sec. The most probable velocities are all within 0-1 km/s in the outward (positive) direction, but these distributions are all broad with $\delta V_{rad} \sim V_{rad}$. The fraction of negative V_{rad} (inward blob velocities) generally decreases at larger radii. Figures 6(c) and 6(d) show the number of blobs in bins of 0.1 in amplitude for each radial zone. Above the minimum level A_{blob} = 1.5, the number of blobs almost always decreases strongly with the blob amplitude.

Figure 7(a) and 7(b) shows the radial velocity of the blobs binned according to their equivalent $\tilde{n}/n=(1-1/A_{blob})$ for both for Ohmic and H-mode plasmas, with only bins having ≥5 blobs shown. Here $\tilde{n}/n=0.33$ corresponds to the minimum level of $A_{blob}=1.5$ and the maximum possible blob level approaches $\tilde{n}/n=1$. The average blob V_{rad} tends to increase with increased $\tilde{n}/n$ over range $\tilde{n}/n \sim 0.33$-1.0, with a particularly clear trend for the H-mode data at +2 cm to +6 cm in the SOL. For example, at a radius of +6 cm the binned radial blob velocity in H-mode increases from V_{rad}~0.5 km/sec at $\tilde{n}/n$~0.4 to V_{rad}

~1.1 at ñ/n~0.9. Note that there were also significant statistical variations in the blob velocity in each bin, shown for example by the standard deviation error bars for selected bins for the +6 cm case in Fig. 7(b). These statistical variations make it difficult to see the trend for increasing V_{rad} with ñ/n when just plotting the individual blobs without binning.

The V_{rad} data for each radial zone in Fig. 7(a) and 7(b) are fit by a power law curve with the power law exponents shown in Table 2, along with R values (correlation coefficients) indicating the quality of the fit. There are strikingly good fits to the H-mode data for radii +2 cm to +6 cm, with power law exponents in the range 3.3 to 1.5 and R~0.93-0.97. However, the Ohmic data over this radial range do not have good power law fits, with R≤0.6. The increasing V_{rad} vs. ñ/n shown in the H-mode data of Fig. 7(b) agrees at least qualitatively the ñ/n dependence of Eq. [3] and [4], but with larger power exponents of ~1.5-4.4 than of those of in these models (i.e. 0.5 or 1.0).

Figure 7(c) and 7(d) shows the radial velocity of the blobs as a function of L_{pol} for Ohmic and H-mode plasmas, binned in increments of 0.1 cm from 2 cm to 10 cm, again using only bins containing ≥ 5 blobs. The average blob V_{rad} tends to decrease with increasing L_{pol} in Ohmic plasmas, but with little or no systematic variation in H-mode (three bins with slightly negative V_{rad} in H-mode at 0 cm and 2 cm are not shown). There is again a large statistical spread within each bin, shown by sample error bars in Fig. 7(c). These V_{rad} vs. L_{pol} variations were also fit by the power law exponents shown in Table 2, along with the R values. There are good power law fits (R≥0.6) to the Ohmic data for radii 0 cm to +4 cm, with power law exponents in the range -0.53 to -0.84. However, the H-mode data do not show any good power law fits, with R≤0.4. The decreasing trend of V_{rad} vs. ñ/n in the Ohmic data of Fig. 7(c) agrees at least qualitatively with the model of Eq. [3], but with smaller exponents than that model (i.e. -2). However, the trends in this data disagree with the model of Eq. [4], which has a +0.5 power law exponent.

An attempt was made to fit all of the whole data set of individual V_{rad} blob speeds jointly with ñ/n and L_{pol} using multiple linear regression analyses for each radial zone,

without the binning as done for Fig. 7. However, no good power law fits were found from any of those regression analyses, i.e. the random variations in the blob data overwhelmed any simple power-law relationship. There was no also significant linear cross-correlation between ñ/n and L_{pol} in any of these cases (R~0.1-0.4), so the trends for V_{rad} vs. ñ/n and L_{pol} in Fig. 7 appear to be independent of each other.

It is interesting that the H-mode data of Fig. 7(d), particularly at +4 and +6 cm, suggests at first an increasing trend with L_{pol}, and then a decreasing trend. This is qualitatively similar to the theory model when the transition from inertial (small blob, $\delta_b < \delta_{b*}$) to sheath-connected (large blob, $\delta_b > \delta_{b*}$) regimes takes place. The observed breakpoint at $L_{pol} \sim 4$ to 5 cm is similar to the expected transition value of $L_{pol} \sim 2\delta_{b*} \sim 3$ to 4 cm for this data. A similar regime transition of blob velocity with poloidal size scale has been previous observed in Torpex [23]. Note that the additional dependences of V_{rad} on c_s and ρ_s (i.e. the T_e in the blob) should also be taken into account in comparisons with theory, but these measurements were not available for individual blobs.

Figure 8 shows a comparison of the radial profile of the measured blob velocities V_{rad} with radial profiles of the calculated V_{sc} and V_{ir} for Ohmic and H-mode plasmas in this database. Here all blobs with amplitude $A_{blob} \geq 1.5$ are averaged together for each radial zone (with their standard deviation shown as an error bar). The average electron temperatures vs. radius from Fig. 1 are used to compute c_s, the average $L_{pol}/2$ vs. radius are used to compute δ_b (see Sec. 8), ñ/n is taken to be the average of $(1\text{-}1/A_{blob})$ for each zone, and R=150 cm and L_{II}=500 cm are assumed for all cases.

The measured V_{rad} for blobs in Ohmic plasmas is within ~0.5-1.0 km/sec, which is roughly consistent (within the joint error bars) with the V_{sc} and V_{ir} in Fig. 8(a), which are in the range ~0.2-2 km/sec. The measured V_{rad} for blobs in H-mode plasmas is within ~0-1 km/s, which is close to V_{sc} in Fig. 8(b), but x5-10 smaller than the estimated V_{ir}. Thus the measured V_{rad} in the SOL are fairly well described by sheath-connected model velocities in both cases, as expected from the blob regime diagram for the SOL in Fig. 2. However, the uncertainties in the theoretical velocities based on uncertainties in c_s, A_{blob},

and L_{pol} are large, especially outside +2 cm where the Thomson data is very uncertain, so this comparison is limited.

7. Poloidal blob velocity

The poloidal velocity of edge turbulence is usually considered to be dominated by the local diamagnetic and/or ExB poloidal flows. However, in the SOL where the fluctuation levels are large, these fluid flows will also be fluctuating in space and time, and blob tilting in theory can also cause blob poloidal motion [31].

Figure 9 shows a comparison of the average poloidal blob velocities V_{pol} vs. radius with the estimated electron diamagnetic and ExB flow velocity for Ohmic and H-mode plasmas in this database. The diamagnetic velocity was taken to be $V_{dia}=c_s\rho_s/L_n$ in the electron direction, and the ExB velocity was estimated by assuming a local SOL potential of $\sim 3T_e$, as expected from connection to the divertor plate sheath (both using B_t in the GPI region). Particularly for the H-modes inside the separatrix, the actual electric field (which was not measured in these discharges) may differ from this estimate. The error bars on the blob velocities are the standard deviations from the blob database, and the error bars for V_{dia} and V_{ExB} were estimated from uncertainties in the Thomson measurements (Fig. 1).

The poloidal ExB velocities in the SOL of ~1-3 km/sec in Fig. 9 are in the same range and direction as the measured poloidal blob velocities for both Ohmic and H-mode cases, at least to within the joint uncertainties. The electron diamagnetic velocities are of the opposite sign, and have considerable uncertainty due to the difficulty in estimating L_n from the Thomson data. In Ohmic plasmas, reversal of the measured blob V_{pol} from the electron diamagnetic direction inside the separatrix to the ExB (i.e. ion direction) in the SOL is commonly seen in other experiments and simulations [31]. When T_i effects are important, as they likely are for the H-mode case here, the ion diamagnetic velocity is

also relevant. Ongoing simulation studies [10] are exploring the relationship of the blob velocity to the diamagnetic and ExB velocities.

The variation of poloidal blob speeds vs. ñ/n = (1-1/A_{blob}) is shown in Fig. 10, binned and plotted similarly to the radial speeds in Fig. 7 and fit with smooth curves (not power laws). For Ohmic plasmas in Fig. 10(a), the blob V_{pol} appears to become increasingly negative (in the ion diamagnetic direction) with increasing ñ/n for radii between +2 to +6 cm, although it is nearly constant vs. ñ/n at 0 cm. This is similar to the behavior of V_{rad} in Fig. 7(a), with the magnitude of both V_{rad} and V_{pol} increasing with ñ/n, and suggests a coupling between V_{rad} and V_{pol} at large ñ/n, which is expected in a general sense from the Reynolds stress mechanism, i.e. fluctuations driven flows. However, this particularly clear experimental demonstration has not (to our knowledge) been previous reported for poloidal blob motion, and is not yet understood in detail (see discussion later in this section). The poloidal velocity in H-mode plasmas at radii of +2 cm and +4 cm in Fig. 10(b) has a maximum in the ion diamagnetic direction for ñ/n~0.5-0.6, which is not expected or understood, as discussed in Sec. 10(b).

The relationship between V_{pol} and V_{rad} for all blobs in the SOL for Ohmic and H-mode plasmas is shown in Fig. 11, along with linear fits to the data in each case. The linear correlation coefficient R between these two quantities is small for the Ohmic cases ($\leq$0.25), as shown in Table 3. However, there is fairly high correlation between these two velocities for the H-mode cases between +2 cm and +4 (~0.54 cm), with V_{pol} becoming closer to zero or more positive (in the electron drift direction) at higher V_{rad}. Surprisingly, at +6 cm V_{pol} becomes more *negative* for larger V_{rad}, although the correlation coefficient is relatively low (0.25).

One possible mechanism for a correlation between V_{pol} and V_{rad} is the tilt angle of the blob charge dipole, which would tend to convert what would have been radial motion into poloidal motion. This effect would be zero for tilts of +90º, for which the major axis of the elliptical blob is in the V_{pol} direction, which is where most of the blob tilts lie (see Fig. 5(f) and the next section). A test of this mechanism was done by re-plotting the data

in Fig. 11 as V_{pol} vs. V_{rad}*cos(tilt), which would show a positive correlation if this mechanism was dominant. However, the cross-correlation coefficients between these two variables were R $\leq$0.4 for all cases, implying that this was not a strong effect in this data. Further constraining the data to A_{blob} >3 did not significantly improve these cross-correlations.

8. Blob structure

The average blob sizes in the poloidal and radial (i.e. vertical and horizontal) directions in GPI images frames like Fig. 3 were plotted Figs. 5(g) and 5(h). These size scales were nearly constant vs. radius within this range, with L_{pol} = 3.6±1.3 cm for Ohmic and L_{pol} = 4.5±1.3 cm for H-mode, and L_{rad} = 2.5±0.8 cm for Ohmic and L_{rad} = 2.4±0.8 cm for H-mode. However, there was a nearly factor-of-two increase in L_{pol} for the innermost radii of -2 cm, perhaps due to the increase in the drift wave parameter ρ_s at higher T_e. There was no significant trend for the blob sizes to increase with the blob amplitudes at any radius, in part due to the definition of blob size as the FWHM of the blob ellipse fit (i.e. not the size at some fixed normalized level).

There is no simple theoretical prediction for the blob size scales, since the blob birth processes are not well understood. However, the turbulence correlation scale lengths at -2 cm over a wide database in NSTX [33] were roughly consistent with k_{pol} ρ_s ~ 0.1 (using the edge B_t), and the blob size data at -2 cm was consistent with that scaling.

Plots of the blob tilt angle vs. ellipticity for Ohmic and H-mode plasmas for various radial zones are shown in Fig. 12, along with linear fits to the data points. Here the ellipticity is defined as the ratio of major to minor radii of the elliptical fits to the blobs, and the tilt angle is the clock-wise angle of the major axis with respect to the radial direction toward the plasma center. The average tilt angles over the range 0-6 cm in the SOL are 89±33º for Ohmic and 100±14º for H-mode plasmas, corresponding to blobs nearly elongated in the poloidal direction (90º). These tilts are qualitatively what would

be expected from the shear in the V_{pol} indicated in Fig. 9 and Fig. 5(f): both less than and greater than 90º in the Ohmic case (i.e. with tilts looking like "\" inside the separatrix and "/" in the near SOL, respectively), and greater than 90º in the H-mode case ("/"). There are no strong variations of tilt with ellipticity, except for a larger spread in tilt for low ellipticities, which is most likely due to uncertainties in the fitting for small ellipticities. There are also no strong variations of tilt or ellipticity with normalized blob amplitude in this database.

The relationship of the blob shape and tilt to the edge sheared flows in NSTX was previously discussed in [31]. Since there were no direct measurements in NSTX of the edge Reynolds stress from the fluctuating local fluid velocities $R=<\delta v_{pol}\, \delta v_{rad}>$ (e.g. from probes or spectroscopy), a "Reynolds stress proxy" (RSP) was developed in the paper cited above to estimate the local Reynolds stress based on the blob structure itself:

$$RSP = -(\sin 2*tilt)(1-ellipticity^2) \qquad [1]$$

where the tilt angle and ellipticity are defined as above.

Figure 13 shows the radial profile of RSP for all blobs for (a) Ohmic and (b) H-mode plasmas and with smoothed fits to this data (magenta lines), along with the average V_{pol} profiles. First, it is significant that nearly the full range of RSP values (−1 to 1) is attained, particularly for the Ohmic case. This indicates that significant shearing stresses are acting on the blobs. The large spread in instantaneous RSP values at a particular radius is suggestive of fluctuating zonal flows. Theoretically, the dimensionless shearing parameter $V_{pol}'\tau$ provides a simple estimate of when local ExB shear significantly affects blob tilt and ellipticity. Here V_{pol}' is the background shearing rate and $\tau \sim L_{rad}/V_{rad}$. For the Ohmic data presented in Fig. 13(a) we estimate a maximum shearing rate just inside the separatrix of $V_{pol}' \sim 1.5 \times 10^5$ /s and $\tau \sim 10^{-5}$ s resulting in $V_{pol}'\tau > 1$ consistent with significant shearing effects. From radial force balance, Reynolds stress drives poloidal flows and we expect that flow should be driven in the direction of $-\partial_x(RSP)$. This is consistent with the negative dip in V_{pol} in Fig. 13(a) between the radii −3 and 0 cm where the RSP variation is most pronounced. Qualitatively, these RSP-related

observations are similar to those reported on in [31] for another NSTX Ohmic discharge. They suggest that in the Ohmic case sheared flows both affect and are affected by the blobs.

The present dataset also allows a similar analysis of an H-mode case, which was not attempted in [31]. Fig. 13(b) shows slightly less total variation in the RSP. We estimate a maximum shearing rate at +2 cm of $V_{pol}{}'$ ~ 1.2 x 10^5 /s and $\tau \sim 4 \times 10^{-5}$ s again resulting in $V_{pol}{}'\tau > 1$ and the implication of significant shearing effects on the blobs at this location. The most significant spatial gradient of the RSP is in the range +3 to +7 cm. The sign of the gradient implies that Reynold's flows should be driven in the positive V_{pol} direction, but this is not observed. Similarly, there is no positive correlation between the RSP gradient and the flow in the range 7 to 10 cm. This suggest that some mechanism other than Reynolds stress dominates flow drive. Inside the separatrix, there may be too few H-mode blobs to make reliable statements. Theoretically, Reynolds driven flows might be expected to be subdominant relative to mean pressure-gradient driven ExB flows, and in the SOL to sheath driven ExB flows. In summary the Ohmic RSP data suggests that blobs and flows mutually affect each other, while the H-mode data suggests that flows affect the tilting of the blobs, but the blobs do not dominate the creation of the flows.

9. Blob SOL width

One potential result of blob structure and motion is a broadening of the scrape-off layer (SOL) width of particles and heat due to outward blob motion across the separatrix. Recently there have been many experimental [e.g. 35,36] and theoretical [e.g. 37,38] studies of the SOL width of tokamaks, motivated mainly by the high divertor plate heat flux expected in ITER. At present it is not clear what mechanisms determine the SOL width in present devices.

The simplest model for the *blob contribution* to the density SOL width assumes that blobs move radially outward at a speed V_{rad} across the separatrix, and that they carry with them all the ions within the blob. If this assumption is true, then the radial distance over which these blob ions move into the SOL is therefore:

$$\lambda_n \sim V_{rad}\, \tau_{blob} \qquad [5]$$

where τ_{blob} is the lifetime of the blobs in the SOL. However, at the same time that the blobs are moving radially in the SOL, the blob ions are also moving along the B field line to the divertor plates, where they eventually are eventually absorbed (or recycled). For the present database, the average lifetime of blobs in the GPI field of view (see Fig. 3) is $\tau_{blob} \sim 23$ μsec for the Ohmic cases and $\tau_{blob} \sim 36$ μsec for the H-mode cases, most of which is spent in the SOL. This is significantly less than the timescale for parallel ion motion along B of $\tau_{sol} \sim 2L_{II}/c_s \sim 500$ μsec, assuming an ion speed of $V_{i,II} \sim c_s/2 \sim 10^6$ cm/sec and a parallel connection length $L_{II} \sim 500$ cm. Thus τ_{blob} is used in Eq. [5] instead of τ_{sol}.

For a typical blob radial velocity of $V_{rad} \sim 0.5$ km/sec in the SOL (see Fig. 5(d)) and a typical blob lifetime of $\tau_{blob} \sim 30$ μsec, the resulting estimate of the blob-induced density SOL width from Eq. [5] is $\lambda_n \sim 1.5$ cm. This within a factor-of-two of the density decay scale length measured by Thomson scattering just outside the separatrix in these experiments as shown in Fig. 1(f); namely, $\lambda_n \sim 3$ cm for the Ohmic case and the $\lambda_n \sim 1$ cm for the H-mode case. This level of agreement is as good as can be expected, considering the many factors not taken into account in this simple analysis; for example, the ionization and recycling source in the SOL, the ion neoclassical orbit effects and flows, and turbulent (non-blobby) particle diffusion into the SOL.

The simplest model for the effect of blobs on the SOL electron temperature width assumes electrons are transported radially at V_{rad} along with the blob density, and that their heat content diffuses along B to the divertor plate due to the competition between

electron thermal motion and collisions. The resulting electron temperature SOL width due to blobs is:

$$\lambda_{Te} \sim V_{rad}\, \tau_{II,e} \qquad [6]$$

The parallel electron heat conduction time $\tau_{II,e} = 3/2 L_{II}^2/\chi_{II,e}$ [35] depends on the electron thermal conductivity $\chi_{II,e}$, and for the separatrix conditions here is roughly $\tau_{II,e} \sim 20$ μsec. Since this time is (marginally) less than τ_{blob}, the blob lifetime is not dominant in determining λ_{Te} as it was for $\lambda_{n.}$ Assuming $V_{rad} \sim 0.5$ km/sec, the blob-induced electron temperature SOL width is thus $\lambda_{Te} \sim 1$ cm, which is x2-3 lower than the measured T_e scale lengths of $\lambda_{Te} \sim$ 2-3 cm at the separatrix as shown in Fig. 1(c). There are again several reasons why Eq. [6] should not be an accurate estimate of the temperature SOL width; for example, the collisional electron heat transport along B may be limited by other processes [35], there may be significant electron energy loss due to radiation in the SOL, and some of the radial electron heat flux may be is due to broadband turbulence rather than blobs.

Note that the SOL width estimates of Eq. [3] and [4] apply only to the *blob-like* components of the radial particle and heat flux, and do not imply that *all* radial fluxes in the SOL are due to blobs. More direct measurements of blob transport have been made using Langmuir probes to directly measure the density and temperature of the blobs [32,39-41], with the general result that blobs appear to contribute significantly to particle and heat transport in the SOL of tokamaks. However, some assumptions are still needed for these estimates, e.g. about the poloidal distribution of the blob-induced transport.

Estimates of the heat flux width, λ_q were made for the H-mode cases from measurements of the divertor heat flux via infrared thermography [42] using a fast (1.6 kHz) IR camera [43]. The radial heat flux profiles in these discharges are highly structured, resulting in a profile that is poorly described by the semi-empirical Diffusive-Gaussian model [36]. Because of this, the FWHM of the near-SOL heat flux profile is used to estimate the heat flux width by averaging 20 frames (12.5 ms) of thermography

data about the time of interest. The divertor heat flux width $\lambda_{q,\,FWHM}^{div}$ is found to range from 88-116 mm in these discharges. When magnetically mapped to the outer midplane, the magnetic flux expansion, f_x, is $11.3 \leq f_x \leq 12.6$ as calculated from EFIT02 reconstructions and averaged spatially 5 mm radially outward from the outer strike point and temporally over the same 12.5 ms as the heat flux profiles. This leads to an inferred midplane heat flux width of $\lambda_{q,\,FWHM}^{mid}$ =7.2 – 10.2 mm, which is in reasonable agreement with other upstream quantities and with the SOL heat flux widths inferred for blobs above.

10. Summary and discussion

Section 10(a) summarizes the results of this paper, Sec. 10(b) discusses some open physics issues concerning the 2-D blob velocity, Sec. 10(c) discusses the definition of a blob, Sec. 10(d) describes comparisons with previous experiments, and Sec. 10(e) esuggests directions for further experiments.

a) Summary

This paper described the 2-D radial vs. poloidal blob structure and motion in the edge and SOL of NSTX for representative Ohmic and H-mode discharges, as measured using a gas puff imaging (GPI) diagnostic. A large database was made for these two types of shots with individual blob amplitudes, spatial sizes, shapes, and velocities as a function of radius, which was used for both empirical correlations and comparisons with blob theory. This extends a previous paper on GPI results in NSTX in which only the average blob properties for each shot were described [33].

In general, there was surprisingly little difference between the blob properties in the SOL for Ohmic and H-mode discharges, as illustrated in Fig. 5. Typical average blob velocities in the SOL were $V_{pol} \sim 2\pm1$ km in the ion diamagnetic drift direction and $V_{rad} \sim 0.5\pm0.5$ km/sec in the outward direction, with spatial scales $L_{pol} \sim 4\pm1$ cm and $L_{rad} \sim 2.5\pm1$ cm. Elliptical fits to the blob structure had ellipticites of ~2±1 and tilt angles

~90º±10º, i.e. with the long axis nearly in the poloidal direction. The clearest difference between Ohmic and H-mode cases was found in the number of blobs detected near or just inside the separatrix, which was much lower in H-mode plasmas than Ohmic plasmas. As usual for blob studies in tokamaks, there was a fairly wide scatter in the individual blob properties even for a given shot and radial zone, as illustrated in Figs. 4-6.

There was a clear trend for the blob V_{rad} in H-mode plasmas to increase with blob amplitude (i.e. $\tilde{n}/n$) in the binned data of Fig. 7(b), and for V_{rad} to decrease with the blob poloidal size scale L_{pol} in Ohmic plasmas in the binned data in Fig. 7(c). These trends were less clear in the un-binned database due to the large scatter in V_{rad}. The power law fits to the trends in the binned data (Table 2) were qualitatively consistent with analytic blob theory (Eqs. 3 and 4), but with larger power law exponents. The radial profile of V_{rad} agreed fairly well with the sheath-connected blob model to within the joint uncertainties, as shown in Fig. 8. The blob poloidal velocities were roughly consistent with the expected ExB drift motion in the SOL, as shown in Fig. 9, although there were also some systematic variations of V_{pol} with the blob $\tilde{n}/n$, as shown in Fig. 10.

The empirical relationships between the blob V_{pol} and V_{rad} at various radii did not show strong correlations between these two speeds, as shown in Fig. 11 and Table 3. There was also little or no empirical correlation between the blob tilts and their ellipticity, as illustrated in Fig. 12. Finally, a theoretical model for the Reynolds stress-induced poloidal blob velocity was tested using a Reynolds stress proxy [31], which suggested that sheared flows both affect and are affected by the blobs, at least for the Ohmic cases.

b) Physics of 2-D motion of blobs

Perhaps the most interesting new result in this paper was the systematic increase in the blob radial velocity with increased blob amplitude for the H-mode cases shown in Fig. 7(b). Although such an increase is a robust prediction of blob models such as Eq's. [3] and [4], due to an increase in the blob poloidal electric field with increased blob amplitude, to our knowledge this result was not found in any previous experiments. Also

interesting was the decrease in blob radial velocity with blob poloidal size in Ohmic plasmas as shown in Fig. 7(c), which is also qualitatively consistent with the decrease in local poloidal electric field with blob size in the sheath-connected model of Eq. 3. Fig. 7(d) hints at a non-monotonic dependence of the radial blob velocity on blob poloidal size in H-mode plasmas, which may be suggestive of inertial effects for smaller size blobs.

The poloidal motion of blobs is less clearly defined in the analytic blob theory. Small amplitude blobs should "go with the flow" in the poloidal direction, but in Ref. [31] it was shown that in the Ohmic case the Reynolds stress arising from SOL currents and radial inhomogeneity is of sufficient strength and direction to explain the V_{pol} reversal of blob tracks across the separatrix. If this nonlinear Reynolds mechanism is correct, then it would be expected to drive V_{pol} increasingly negative as A_{blob} increases, apparently consistent with the increase in the (negative) Ohmic V_{pol} at large $A_{blob} > 4$ ($\tilde{n}/n > 0.75$) in Fig. 10(a). On the other hand, Fig. 10(b) shows that for the H-mode cases with $A_{blob} > 4$, $V_{pol} \sim -1$ km/s at all radii. Several mechanisms particular to large amplitude blobs can result in motion in the observed ion diamagnetic direction, such as positive charging and rotation [31,44] or finite ion pressure [8,10,14,45]. However, at present it is not understood why any of these mechanisms would result in a nearly constant V_{pol} for all SOL radii when A_{blob} exceeds a threshold.

c) Definition of a blob

The theoretical concept of an isolated blob in the SOL is well defined and allows straightforward analytic modeling of blob motion [1-3]. However, the blobs observed in tokamak experiments are never completely isolated, so there is no universal definition of a blob in the experimental literature. The blobs in the present paper were defined by a 2-D blob tracking algorithm appropriate for the GPI diagnostic (Sec. 4), but the blobs in 0-D or 1-D measurements are defined differently, e.g. by a 2.5 x rms-level threshold [46], and characterized by a threshold for the skewness or kurtosis of a single-point time series. Thus it is difficult to compare results on blobs across different experiments, for example

with respect to the blob creation process, the blob number density, and blob transport effects.

This lack of clear definition for a blob is not surprising in the context of neutral fluid turbulence, where the analogous concept of a 'coherent structure' is also not well defined despite many years of research [47,48]. Coherent structures can sometimes be seen clearly in fluids, e.g. as tornados in thunderstorms, or "bubble and spike" structures in nonlinear Rayleigh-Taylor instabilities, but usually they are hidden within the complexity of the turbulence. Although the initial search for 'blobs' in a tokamak edge [49] was motivated by coherent structures in fluids, those results were *negative*, in that no clear evidence for 'coherent structure' in plasma blobs was found. In the present paper the strongest evidence for blobs as coherent structures is the degree to which the results in Fig. 7(b) and 7(c) and Fig. 8 agreed qualitatively with analytic blob theory.

Further attempts to understand the role of blobs in the tokamaks edge could attempt to directly compare specific blob measurements with synthetic diagnostics from computational simulations. In that case a unique definition of a blob is not crucial, since multiple aspects of the blob structure and motion can be compared. Clarification of the physics of blobs can be pursued by a detailed comparison of the computational results with the simplified analytic models.

d) Comparison with other tokamak measurements

The properties of blobs in the SOL of tokamaks were summarized in a review in 2011 [3]. There the radially outward blob speed ranged over V_{rad} ~ 0.2-3 km/sec and the poloidal blob size scale ranged over L_{pol} ~ 1-8 cm (FWHM), with a slight tendency for increased speed with increased blob size. The blob properties in the present paper are at the low end of this velocity range and the high end of this size range. Comparisons of the present results with some of the more recent measurements of blobs in tokamaks are summarized below (see also other papers in this Special Issue).

Blob sizes and velocities in the Alcator C-Mod SOL were measured in Ohmic plasmas using 2-D GPI data with a blob tracking algorithm with [50]. Blob sizes were in the range $L_{pol} \sim L_{rad} \sim 0.7$ cm, which is about x4-6 smaller than those in NSTX, most likely due to the 10x larger toroidal field in C-Mod (B=5 T). The radial blob velocities were $V_{rad} \sim 0.1$-0.4 km/sec outward, similar to those in NSTX, while the poloidal blob velocities $V_{pol} \sim 0.1$-0.4 in the ion diamagnetic direction, somewhat lower than those in NSTX. Intermittent fluctuations were also studied in C-Mod using time series of GPI data [51], which showed large amplitude bursts with a fast rise and slow decay, which were characterized by a stochastic model.

Recent measurements of blobs were also done using GPI in the SOL of L-mode and H-mode plasmas in ASDEX upgrade [22]. The average poloidal blob sizes were $L_{pol} \sim 1.5$ cm (FWHM) in Ohmic L-mode and H-mode, with a broad distribution of size scales in both cases. These sizes are about 3x smaller than those in NSTX (e.g. Fig. 5), most likely due to the 5x larger toroidal field in ASDEX (B=2.5 T). The radial blob velocities in ASDEX were $V_{rad} \sim 0.3$ km/sec in both Ohmic L-mode and H-mode, which is similar to the radial blob speeds seen in NSTX. There was a reversal of V_{pol} in Ohmic L-mode plasmas near the separatrix, and a similar blob detection rate in Ohmic than in H-mode, both of which are similar to the NSTX results of Fig. 5. The radial blob velocities were also measured in ASDEX upgrade in L-mode plasmas using a 1-D Li-BES array [52], and these velocities decreased with increased blob size, similarly to the sheath-connected blob model and at least qualitatively similar to the results of Fig. 7(c) here.

Probe measurements of blobs in the SOL of NSTX [32] were generally similar to blobs seen by GPI, as discussed there. Probe measurements of SOL density fluctuations in MAST were recently compared with predictions of the ESEL turbulence code [53], and distributions of the measured radial size and perpendicular velocity of the filaments (i.e. blobs) appear to agree with those of the code. The fluctuations measured using probes in the SOL of TCV [54] were analyzed as a superposition of uncorrelated burst events, such that the average plasma density and fluctuations in the far SOL are due to

the radial motion of blob-like structures. This statistical model appears to be at least qualitatively similar to the picture of blobs provided in the present paper.

e) Experimental directions

There are many possible directions for further experimental work on blobs in the SOL of tokamaks. Of fundamental diagnostic and physics importance would be the direct measurement of the 2-D structure of the density and temperature within blobs, perhaps using the HeI line ratio technique [55]. In addition, it would be valuable to have independent measurements of the SOL plasma flows and electrical currents on a blob timescale, e.g. using Mach probes and magnetic probes [56].

Although some good work has been done on the parallel correlation of SOL turbulence in tokamaks [29,57], it would be highly interesting to image the entire 3D filamentary structure of blobs, e.g. to determine the effect of the X-point region and to examine how blobs connect to the divertor plate. This would most likely require multiple camera views and sophisticated image reconstruction. Finally, it might be possible to develop active blob control techniques to help manage heat and particle removal at the tokamak wall; in particular, if the blob radial velocity can be increased, the SOL width should be increased. To this end, it would be useful to study 'seeded' blobs in the edge of a tokamak using highly localized edge sources, e.g. pulsed electron cyclotron heating or shallow pellets or dust.

Even without additional diagnostics, the analysis of blob structure and motion in the existing 2D imaging data can be significantly improved by allowing a variable blob fitting shape to better track the collisions, merging, and/or splitting of blobs. It is clear from viewsing the movies of the present data [58] that there are many interesting features of blobs in the SOL of NSTX which have not been identified by the present analysis.

Acknowledgments:

We thank for their contributions to this paper and this study in general: J.W. Ahn, S. Banerjee, J.A. Boedo, O.E. Garcia, R.W. Gould, S.I. Krasheninnikov, S. Kubota, R. Maingi, T. Munsat, S. Sabbagh, Y. Sechrest, J.L.Terry. This work was supported by #USDOE Contract DE-AC02-09CH11466 and DE-FG02-02ER54678. The digital data for this paper can be found in http://arks.princeton.edu/ark:/88435/dsp018p58pg29j.

References:

[1] Krasheninnikov SI, Phys. Lett. A 283 (2001) 368
[2] Krasheninnikov SI et al, J. Plasma Phys. **74**, 679 (2008)
[3] D'Ippolito DA et al 2011 Phys. Plasmas **18**, 060501
[4] Ryutov DD Phys. Plasmas 13 (2006) 122307
[5] Walkden NR et al Plasma Phys. Control. Fusion 55 (2013) 105005
[6] Kube R et al, J. Nucl. Mat. 438 (2013) S505
[7] Carralero D. et al Nucl. Fusion 54 (2014) 102307
[8] Bisai N et al, Phys. Plasmas 19 (2012) 052509
[9] Manz P et al, Phys. Plasmas 20 (2013) 022308
[10] Russell D. et al Phys. Plasmas 22 (2015) 092311
[11] Angus JR et al, Phys. Plasmas 19 (2012) 082312, Phys. Plasmas 21 (2014) 112504
[12] Halpern F D et al, Phys. Plasmas 20 (2013) 092308
[13] Easy, L et al, Phys. Plasma 21 (2014) 122515
[14] Madsen J et al, Phys. Plasmas 18 (2011) 112504
[15] Wiesenberger M et al, Phys. Plasmas 21 (2014) 092301
[16] Manz P et al, Phys. Plasmas 22 (2015) 022308
[17] Bodi K et al Phys. Plasmas 15 (2008) 102304
[18] Kendl A Plasma Phys. Control. Fusion 57 (2015) 045012
[19] Anderson J. et al, Phys. Plasmas 21 (2014) 122306
[20] Kube R Phys. Plasmas 22 (2015) 012502
[21] Garcia OE Phys. Rev. Lett. 108 (2012) 265001
[22] Fuchert G et al, Plasma Phys. Control. Fusion 56 (2014) 125001
[23] Theiler C et al Phys. Plasmas 18 (2011) 055901
[24] Katz N et al, Phys. Rev. Lett. 101 (2008) 015003
[25] Zweben SJ et al 2004 Nucl. Fusion **44**, 134
[26] Myra JR et al 2006 Phys. Plasmas **13** 092509
[27] Myra JR et al 2011 Phys. Plasmas **18** 012305
[28] Russell DA et al 2011 Phys. Plasmas **18** 022306
[29] Maqueda, R et al, Nucl. Fusion 50 (2010) 075002
[30] Maqueda RJ et al 2011 J. Nucl. Mat. **415**, S459
[31] Myra JR et al 2013 Nucl. Fusion **53** 073013
[32] Boedo J et al, Phys. Plasmas 21 (2014) 042309
[33] Zweben SJ et al, Nucl. Fusion 55 (2015) 093035
[34] Zweben SJ et al, Plasma Phys. Control. Fusion 56 (2014) 095010
[35] Fundamenski W et al Nucl. Fusion **47** (2007) 417
[36] Eich T et al Phys. Rev. Lett. 107, 215001
[37] Ricci P et al, Phys. Plasmas 20 (2013) 010702
[38] Myra JR et al, Phys. Plasmas 22 (2015) 042516
[39] Boedo J et al, Phys. Plasmas 8 (2001) 4826
[40] Simon P et al, Plasma Phys. Control. Fusion 56 (2014) 095015
[41] Ionita C et al, Nucl. Fusion 53 (2013) 043021
[42] Gray TK et al J. Nucl. Mat. 415 (2011) S360–S364
[43] Mclean AG et al Rev. Sci. Instrum. **83** (2012) 053706
[44] Furno I et al, Phys. Plasmas 53 (2011) 124016

[45] Jovanovic D et al Phys. Plasmas 15 (2008) 112305
[46] Boedo JA, Phys. Plasmas 10 (2003), 1670
[47] Ouelette NT Comptes Rendus Physique 13 (2012) 866
[48] Peacock, T, Haller, G., Physics Today, 41 (2013)
[49] Zweben SJ Phys. Fluids 28 (1985) 974
[50] Kube R et al, J. Nucl. Mat. 438 (2013) S505
[51] Garcia OE et al, Phys. Plasmas 20 (2013) 055901
[52] Birkenmeier G et al, Plasma Phys. Control. Fusion 56 (2014) 075019
[53] Militello P et al, Plasma Phys. Control. Fusion 55 (2013) 025005
[54] Garcia OE et al, Nucl. Fusion 55 (2015) 062002
[55] Agostini M et al, Plasma Phys. Cont. Fusion 51 (2009) 105003
[56] Spolaore, M et al, Phys. Plasmas 22, 012310 (2015)
[57] Grulke O et al, Nucl. Fusion 54 (2014) 043012
[58] see http://w3.pppl.gov/~szweben/PPCFblob/PPCFblob.html

Table 1: Parameters for this database

	Ohmic	H-mode
shot range	141746-756	140389-395
time range (sec)	0.213-0.214	0.535-0.550
I_p (kA)	830	830
B_t (kG)	3.6	4.9
kappa (elongation)	1.9	2.4
W_{mhd} (kJ)	32	220
n_e average (10^{13} cm^{-3})	1.6	5.2
P_{nb} (MW)	0	4.0
$T_e(0)$ (eV)	530	920
$n_e(0)$ (10^{13} cm^{-3})	2.3	5.6
$T_e(a)$ (eV)	13±6	29±17
$n_e(a)$ (10^{13} cm^{-3})	0.37±0.23	0.92±0.54
T_e @ -2 cm (eV)	23±4	134±53
n_e @ -2 cm (10^{13} cm^{-3})	0.47±0.17	2.1±0.47
ρ_s (cm) @ -2 cm	0.2	0.3
τ_{ei} (μsec) @ -2 cm	0.5	1.5
β_e @ -2 cm	0.0003	0.005
# of blobs identified	28,800	18,800
# of blob trails	2600	820
blob trail lifetime (μs)	23	36

Table 2: Blob radial velocity vs. ñ/n and L_{pol} (power law and R values)

	Vrad vs. ñ/n Ohmic	Vrad vs. ñ/n H-mode	Vrad vs. Lpol Ohmic	Vrad vs. Lpol H-mode
0 cm	1.50 (0.73)	4.4 (0.92)	-0.84 (0.65)	-0.58 (0.29)
+2 cm	0.10 (0.15)	3.3 (0.97)	-0.67 (0.81)	0.29 (0.10)
+4 cm	0.32 (0.60)	1.7 (0.95)	-0.53 (0.76)	-0.20 (0.36)
+6 cm	0.44 (0.53)	1.5 (0.93)	-0.33 (0.55)	-0.22 (0.25)

Table 3: Linear fit coefficients of V_{pol} vs. V_{rad} (R values in parentheses)

	Ohmic	H-mode
0 cm	0.60 (0.21)	1.1 (0.53)
+2 cm	0.28 (0.13)	2.1 (0.52)
+4 cm	0.06 (0.03)	2.1 (0.56)
+6 cm	-0.030 (0.02)	-0.31 (0.25)

Figures

Fig. 1 - In (a) and (d) are the profiles of n_e and T_e from Thomson scattering for the H-mode and Ohmic discharges in this paper, averaged over the 7 shots of each type. In (b) and (e) are the radial gradients of these n_e and T_e profiles, and in (c) and (f) are the radial n_e and T_e scale lengths. The error bars represent the shot-to-shot standard deviations.

Fig. 2 – Regime diagram for blob propagation in the parameter space of the collisionality parameter Λ and blob size Θ (see text for definitions). Regimes are: inertial (IN), resistive X-point (RX), sheath connected (SC) and sheath interchange (CI) (see [26] for details). Ohmic (blue) and H-mode (red) data are shown for parameters characteristic of the separatrix, i.e. at 0 cm ("Sep") and of the far SOL, at 6 cm ("SOL").

Fig. 3 – Sample blob trails in the GPI radial vs. poloidal plane for an Ohmic shot (left, #141746) and H-mode shot (right, #140395), showing all blobs in a 1 msec period for Ohmic and a 2 msec period for H-mode. The ellipticity and tilt of the initial location of each blob is shown by the ellipses (but the size is not drawn to scale). More blobs are born inside the separatrix (dashed lines) in Ohmic plasmas than in H-mode. The RF limiter shadow is shown by the dotted line. Blob quantities are defined at the right.

Fig. 4 – All blobs from the database for Ohmic (left) and H-mode (right) discharges, plotted with respect to the distance from the local separatrix. Parts (a) and (b) show the normalized blob amplitudes, parts (c) and (d) show the radial blob velocities (km/sec), and parts (e) and (f) show the poloidal blob velocities (km/sec). There is a large spread in these blob properties at each radius, but also some systematic trends vs. radius.

Fig. 5 - Average blob properties for Ohmic (blue) and H-mode (red) plasmas as a function of distance from the local separatrix. Part (a) shows the number of blobs per frame N_{blob}, part (b) shows the normalized blob amplitude A_{blob}, parts (c) and (d) show the blob poloidal and radial velocities V_{pol} and V_{rad} in km/sec, parts (e) and (f) show the blob ellipticity and tilt angle (in degrees), and parts (g) and (h) show the blob poloidal

and radial scale lengths L_{pol} and L_{rad} (FWHM). Except for the blob number distribution, the average blob properties in the SOL are similar between the Ohmic and H-mode cases.

Fig. 6 - Distribution of the number of blobs in various radial zones as a function of the blob radial velocity in (a) Ohmic and (b) H-mode, and as a function of the blob amplitude in (c) Ohmic and (d) H-mode plasmas. The radial velocity distributions V_{rad} are always broad, with average outward (positive) velocities in all cases, but with a significant number of inward velocities, especially near the separatrix. The number of blobs is generally a strongly decreasing function of the amplitude A_{blob}.

Fig. 7 - Blob radial velocity vs. equivalent blob fluctuation level $\tilde{n}/n=1-1/A_{blob}$ for (a) Ohmic and (b) H-mode plasmas, binned in units of 0.1 in $\tilde{n}/n$. Part (b) shows a clear trend for V_{rad} to increase with $\tilde{n}/n$ for H-mode plasmas. The blob radial velocity vs. L_{pol} are shown in parts (c) for Ohmic and (d) for H-mode, binned in units of 0.1 cm in L_{pol}. Part (c) shows a clear trend for V_{rad} to decrease with L_{pol} for Ohmic plasmas. Each set of data is fit by a power law curve with exponents shown in Table 2, and standard deviations of the blob distributions in selected bins are shown as error bars in (b) and (c).

Fig. 8 - Comparison of average blob radial velocity vs. analytic models for sheath connected (sc) and inertial (in) for (a) Ohmic and (b) H-mode plasmas. The measured radial blob velocities are generally similar to the sheath-connected model velocities but lower than inertial velocities, although there are significant uncertainties in the model estimates, especially in the SOL.

Fig. 9 - Comparison of the average blob poloidal velocity vs. analytic models for the poloidal electron diamagnetic flow speed V_{dia} and the poloidal ExB flow speed V_{ExB}. The measured poloidal blob velocities are in the ion diamagnetic direction in the SOL and close to those expected from the V_{ExB} due to the sheath potential (estimated from the T_e gradient).

Fig. 10 - Blob poloidal velocity V_{pol} vs. blob fluctuation level ñ/n=1-1/A_{blob} for (a) Ohmic and (b) H-mode plasmas, binned in units of 0.1 in ñ/n. There is a trend for V_{pol} to become increasingly negative for high ñ/n in Ohmic plasmas for radii from +2 to +6 cm, and for V_{pol} for H-mode plasmas to peak in the negative direction near ñ/n~0.5-0.6.

Fig. 11 – Poloidal blob velocity V_{pol} vs. radial blob velocity V_{rad} for radial zones in the SOL, with Ohmic plasmas at the left and H-mode plasmas at the right, along with linear fit lines in blue. There is little correlation of V_{pol} and V_{rad} for the Ohmic cases, as shown by the R values in Table 3, but there is a moderate correlation of V_{pol} and V_{rad} for the H-mode cases at 0 cm to +4 cm.

Fig. 12 - Plots of the blob tilt angle vs. ellipticity for Ohmic (left) and H-mode (right) for various radial zones in the SOL, along with linear fits in blue (tilt is defined in Fig. 3). The average tilt angles are near 90º (black lines), corresponding to blobs elongated in the poloidal direction. There is little or no systematic variation of tilt with ellipticity.

Fig. 13 - Radial profiles of the Reynolds stress proxy (RSP) for all (a) Ohmic and (b) H-mode plasmas, along with smoothed fits to the RSP data (purple lines) and the average blob V_{pol} profiles (in units of km/sec/10). The Ohmic RSP data suggests that blobs and flows mutually affect each other, while the H-mode data suggests that flows affect the tilting of the blobs, but the blobs do not dominate the creation of the flows.

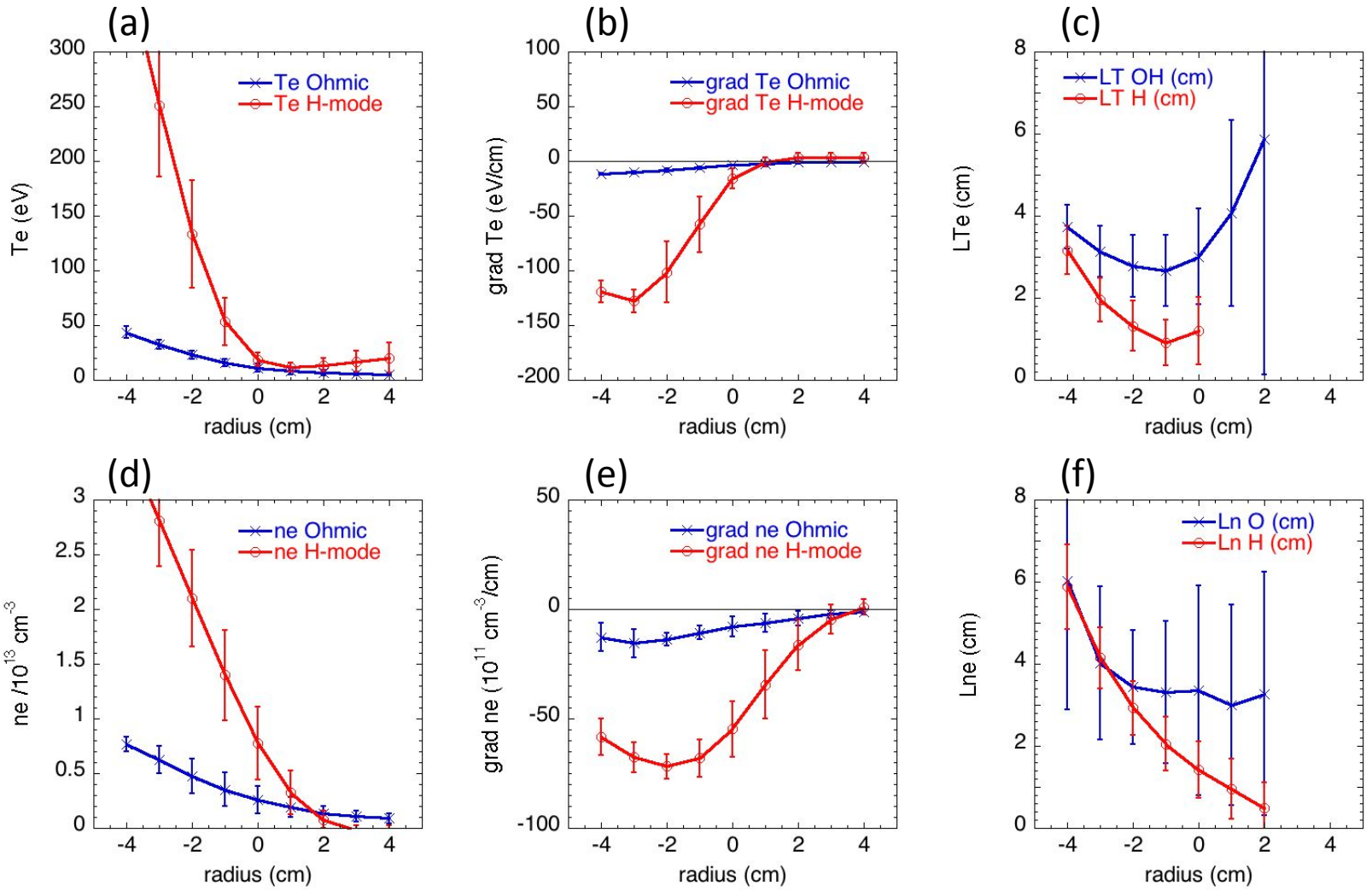
(a)
Te Ohmic
Te H-mode
Te (eV)
radius (cm)
(b)
grad Te Ohmic
grad Te H-mode
grad Te (eV/cm)
radius (cm)
(c)
LT OH (cm)
LT H (cm)
LTe (cm)
radius (cm)
(d)
ne Ohmic
ne H-mode
ne /10^13 cm^-3
radius (cm)
(e)
grad ne Ohmic
grad ne H-mode
grad ne (10^11 cm^-3/cm)
radius (cm)
(f)
Ln O (cm)
Ln H (cm)
Lne (cm)
radius (cm)

Fig. 1

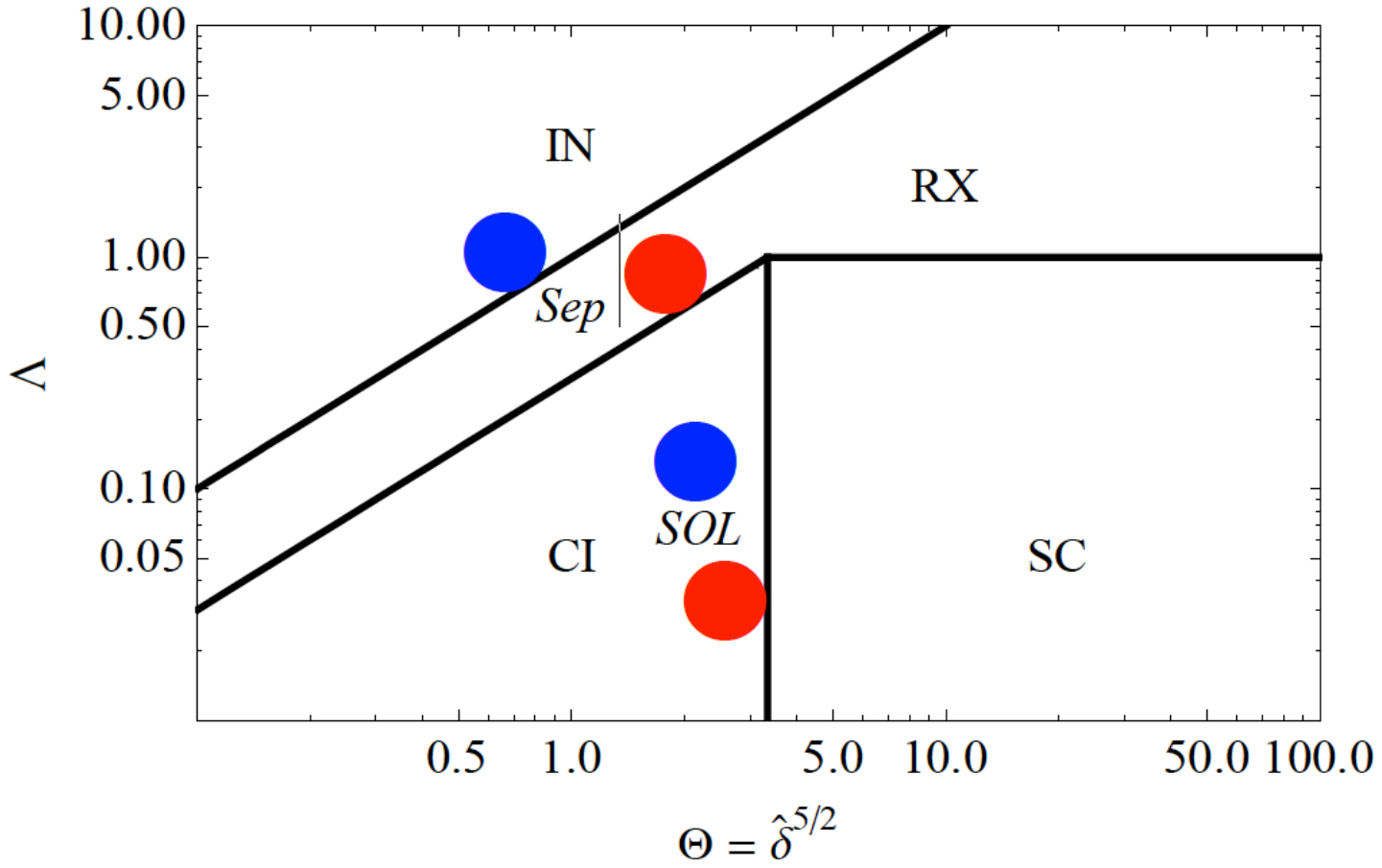
10.00
5.00
1.00
0.50
0.10
0.05
Λ
IN
RX
Sep
SOL
CI
SC
0.5
1.0
5.0
10.0
50.0
100.0
$\Theta = \hat{\delta}^{5/2}$

Fig. 2

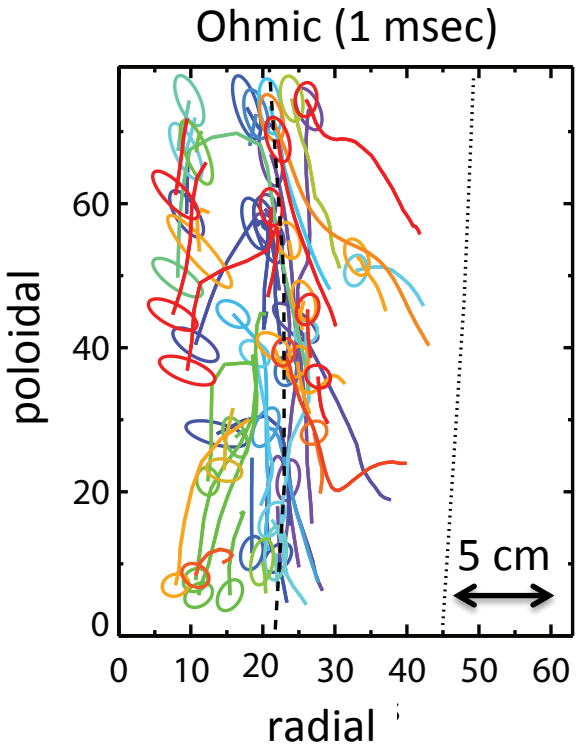
Ohmic (1 msec)
poloidal
radial
0
20
40
60
0
10
20
30
40
50
60
5 cm

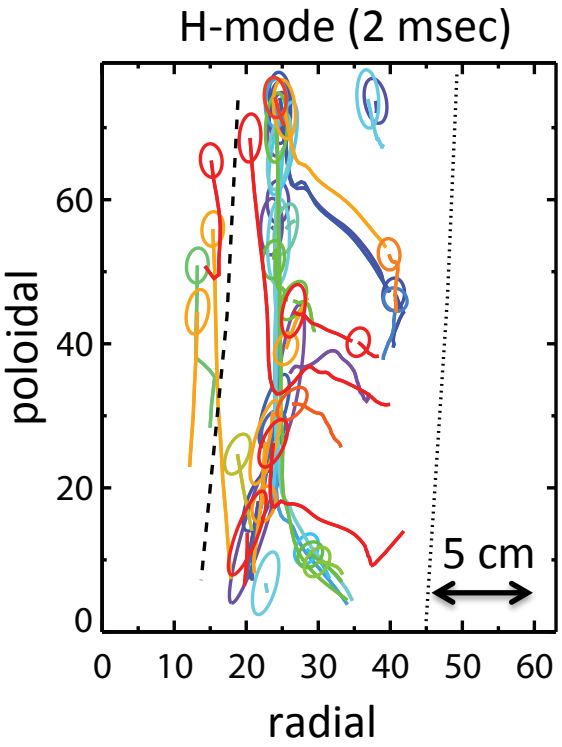
H-mode (2 msec)
poloidal
radial
0
20
40
60
0
10
20
30
40
50
60
5 cm

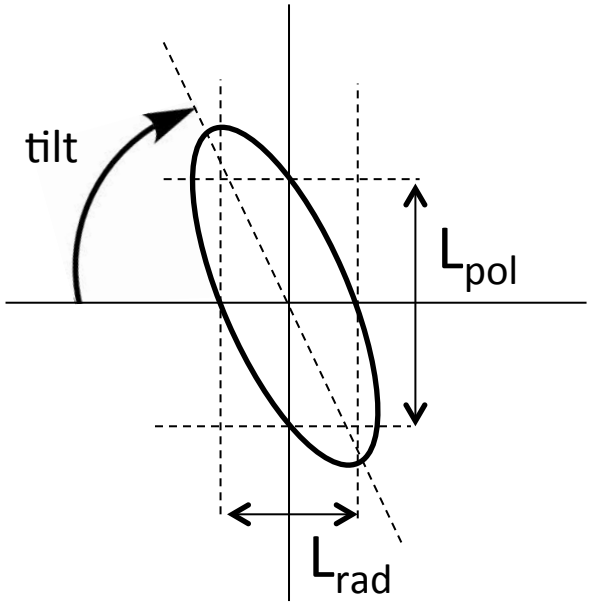
tilt
L_{pol}
L_{rad}

Fig. 3

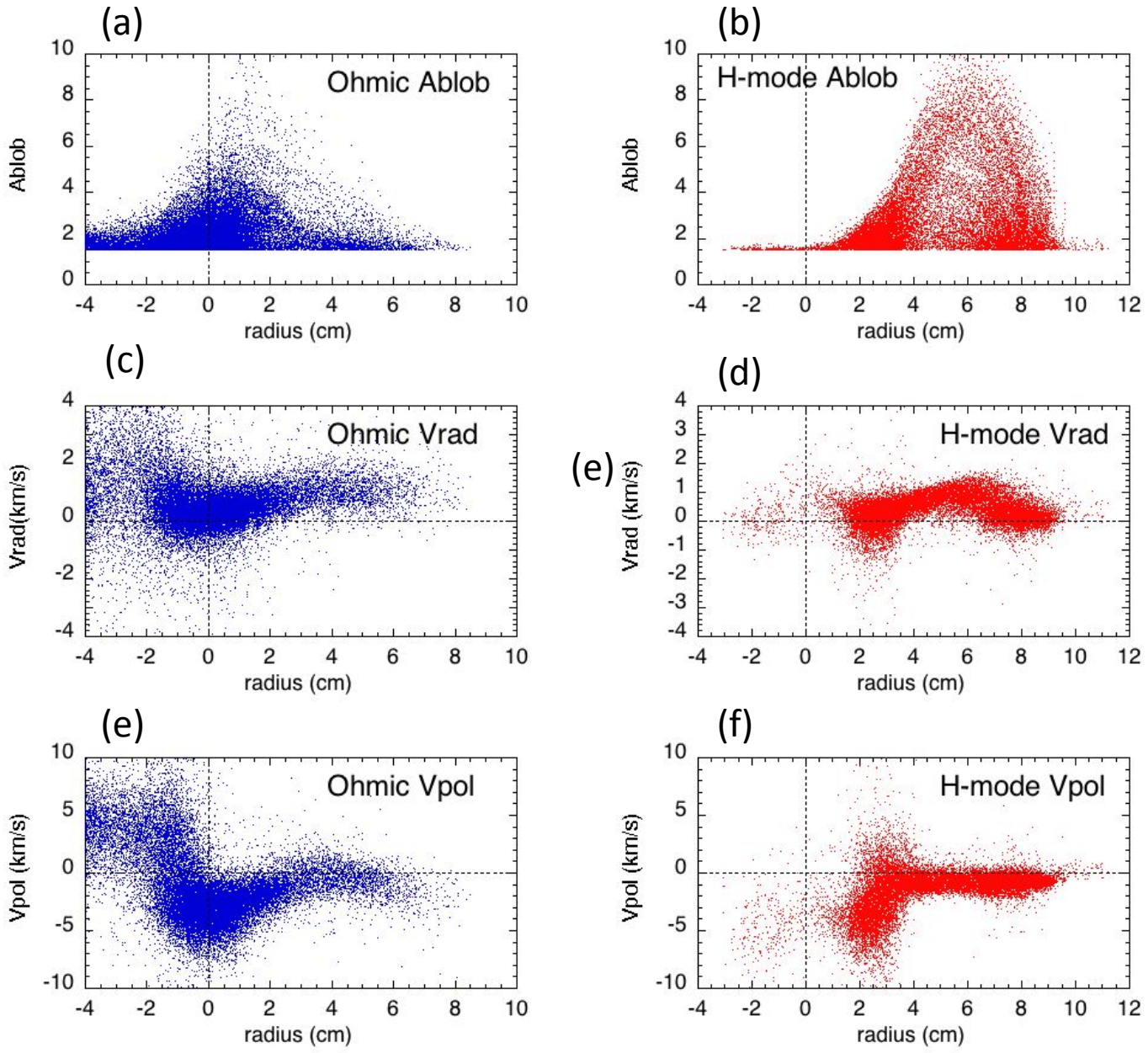
(a)
Ohmic Ablob
Ablob
radius (cm)
(b)
H-mode Ablob
Ablob
radius (cm)
(c)
Ohmic Vrad
Vrad(km/s)
radius (cm)
(d)
H-mode Vrad
Vrad (km/s)
radius (cm)
(e)
Ohmic Vpol
Vpol (km/s)
radius (cm)
(f)
H-mode Vpol
Vpol (km/s)
radius (cm)

Fig. 4

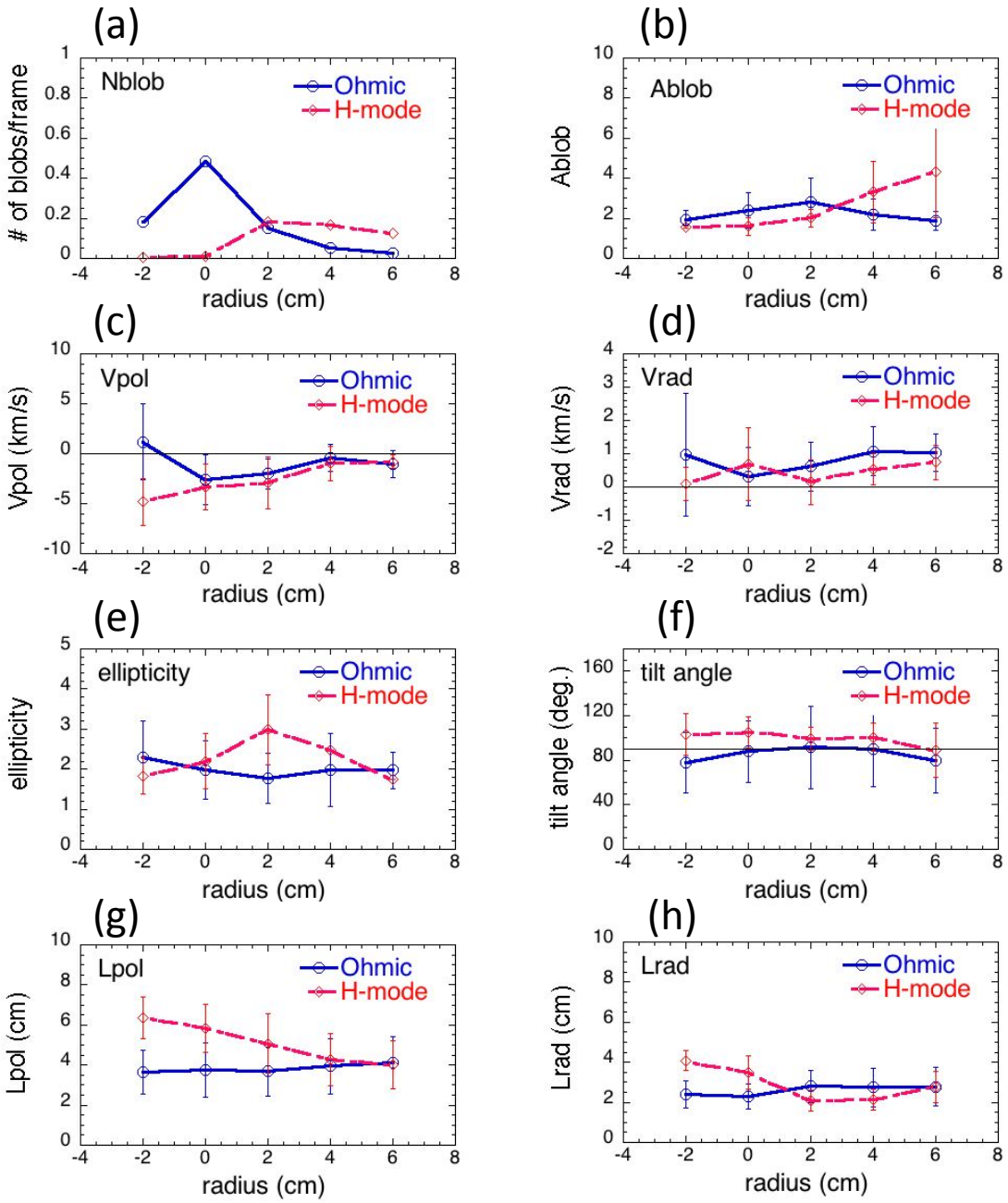
(a)
Nblob
Ohmic
H-mode
# of blobs/frame
radius (cm)
(b)
Ablob
Ohmic
H-mode
Ablob
radius (cm)
(c)
Vpol
Ohmic
H-mode
Vpol (km/s)
radius (cm)
(d)
Vrad
Ohmic
H-mode
Vrad (km/s)
radius (cm)
(e)
ellipticity
Ohmic
H-mode
ellipticity
radius (cm)
(f)
tilt angle
Ohmic
H-mode
tilt angle (deg.)
radius (cm)
(g)
Lpol
Ohmic
H-mode
Lpol (cm)
radius (cm)
(h)
Lrad
Ohmic
H-mode
Lrad (cm)
radius (cm)

Fig. 5

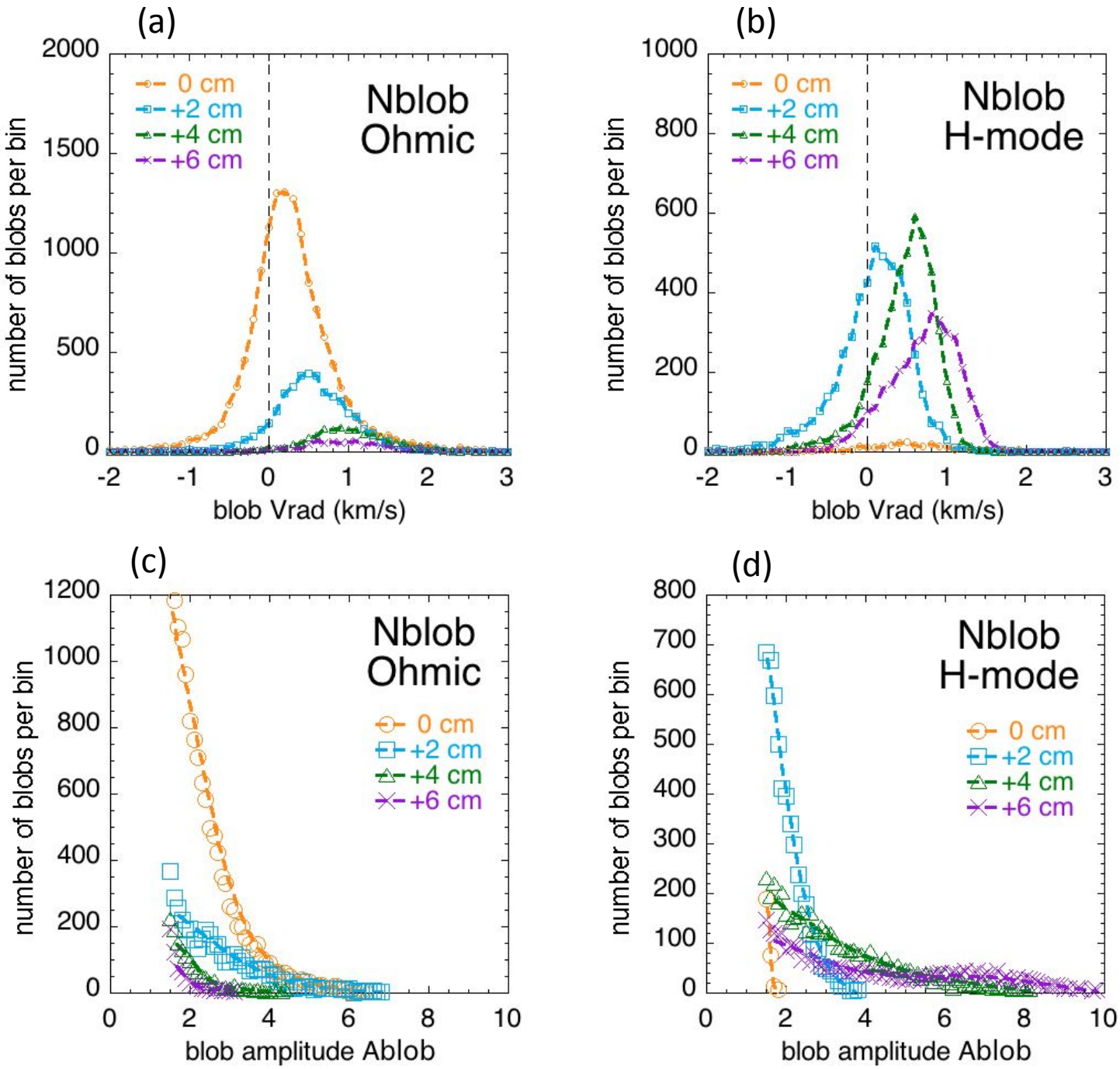
(a)
Nblob
Ohmic
0 cm
+2 cm
+4 cm
+6 cm
number of blobs per bin
blob Vrad (km/s)
(b)
Nblob
H-mode
0 cm
+2 cm
+4 cm
+6 cm
number of blobs per bin
blob Vrad (km/s)
(c)
Nblob
Ohmic
0 cm
+2 cm
+4 cm
+6 cm
number of blobs per bin
blob amplitude Ablob
(d)
Nblob
H-mode
0 cm
+2 cm
+4 cm
+6 cm
number of blobs per bin
blob amplitude Ablob

Fig. 6

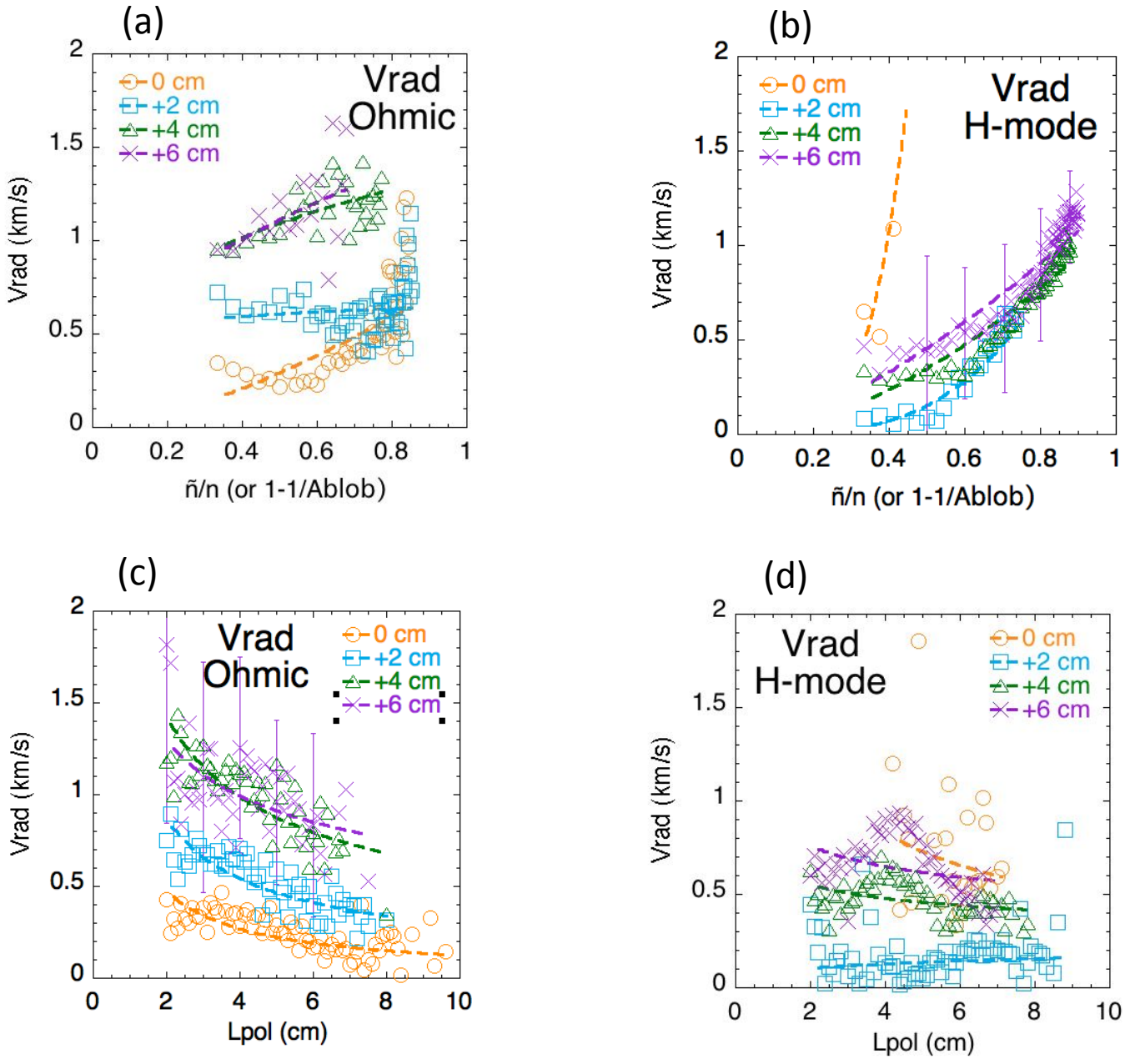
(a)
Vrad
Ohmic
0 cm
+2 cm
+4 cm
+6 cm
Vrad (km/s)
ñ/n (or 1-1/Ablob)
(b)
Vrad
H-mode
0 cm
+2 cm
+4 cm
+6 cm
Vrad (km/s)
ñ/n (or 1-1/Ablob)
(c)
Vrad
Ohmic
0 cm
+2 cm
+4 cm
+6 cm
Vrad (km/s)
Lpol (cm)
(d)
Vrad
H-mode
0 cm
+2 cm
+4 cm
+6 cm
Vrad (km/s)
Lpol (cm)

Fig. 7

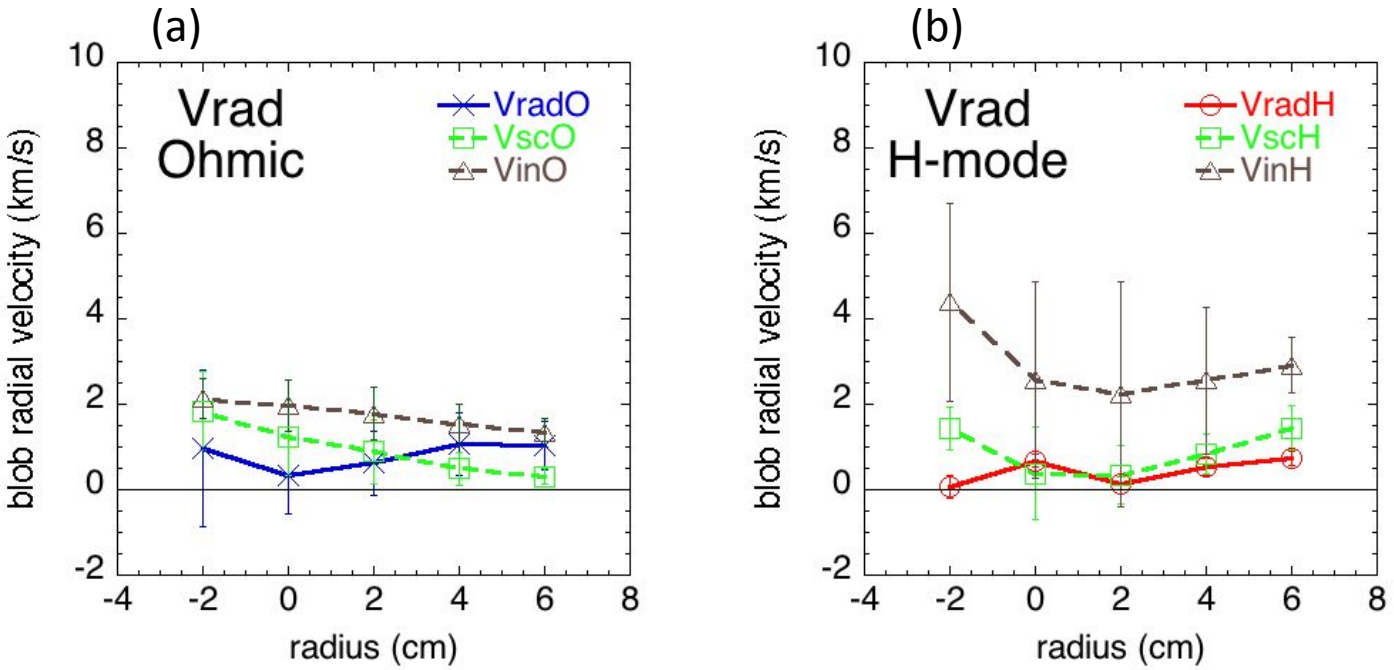
(a)
Vrad
Ohmic
VradO
VscO
VinO
blob radial velocity (km/s)
radius (cm)
(b)
Vrad
H-mode
VradH
VscH
VinH
blob radial velocity (km/s)
radius (cm)

Fig. 8

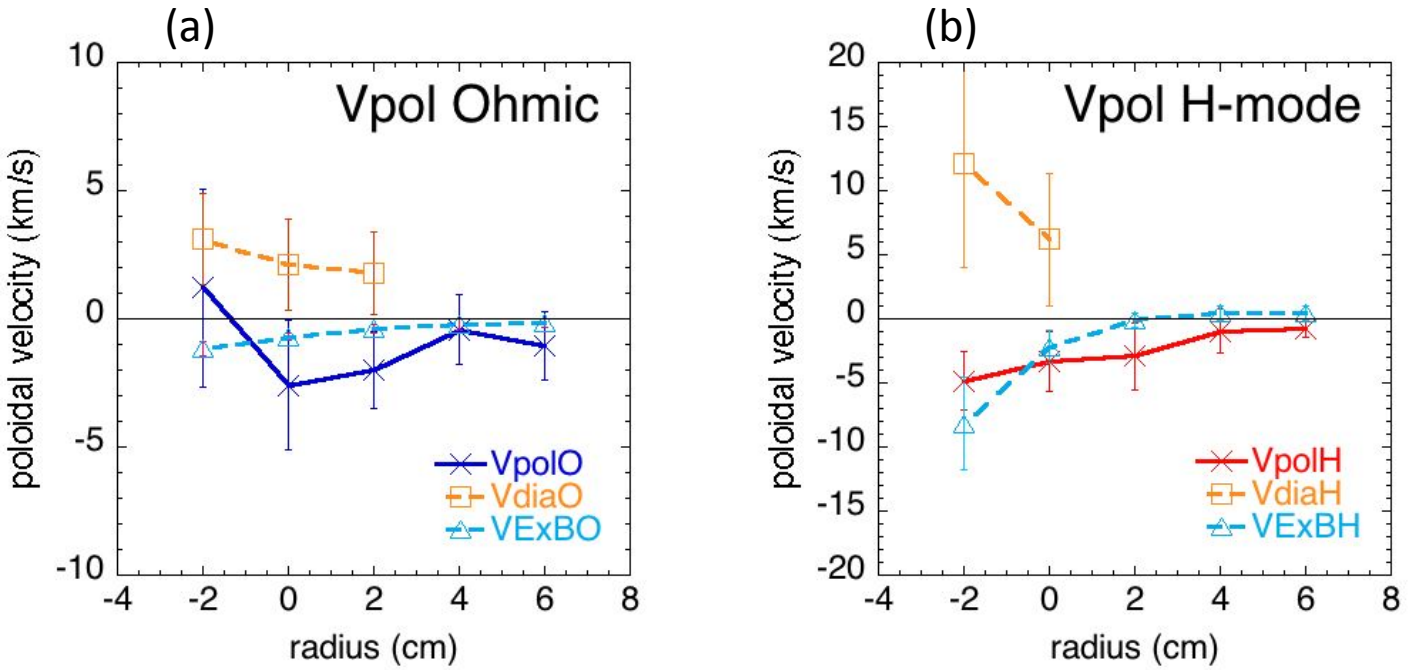
(a)
Vpol Ohmic
poloidal velocity (km/s)
radius (cm)
VpolO
VdiaO
VExBO
(b)
Vpol H-mode
poloidal velocity (km/s)
radius (cm)
VpolH
VdiaH
VExBH

Fig. 9

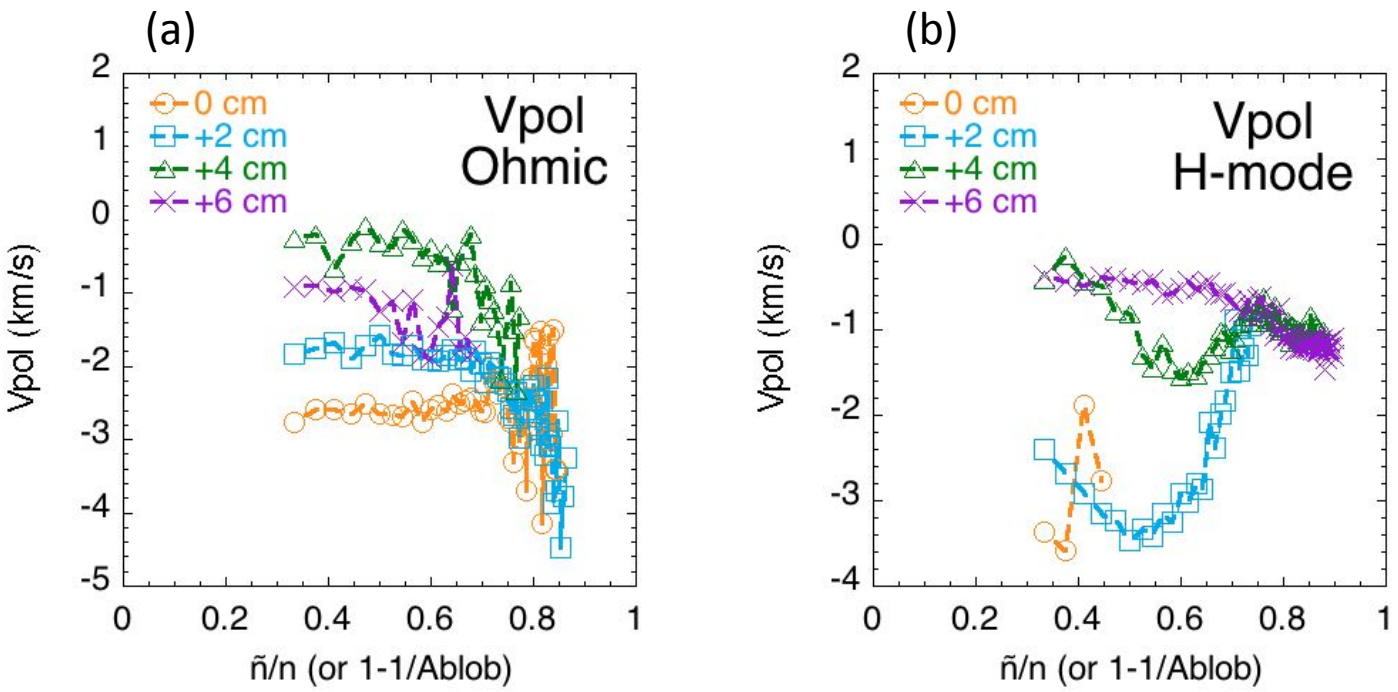
(a)
0 cm
+2 cm
+4 cm
+6 cm
Vpol
Ohmic
Vpol (km/s)
ñ/n (or 1-1/Ablob)
(b)
0 cm
+2 cm
+4 cm
+6 cm
Vpol
H-mode
Vpol (km/s)
ñ/n (or 1-1/Ablob)

Fig. 10

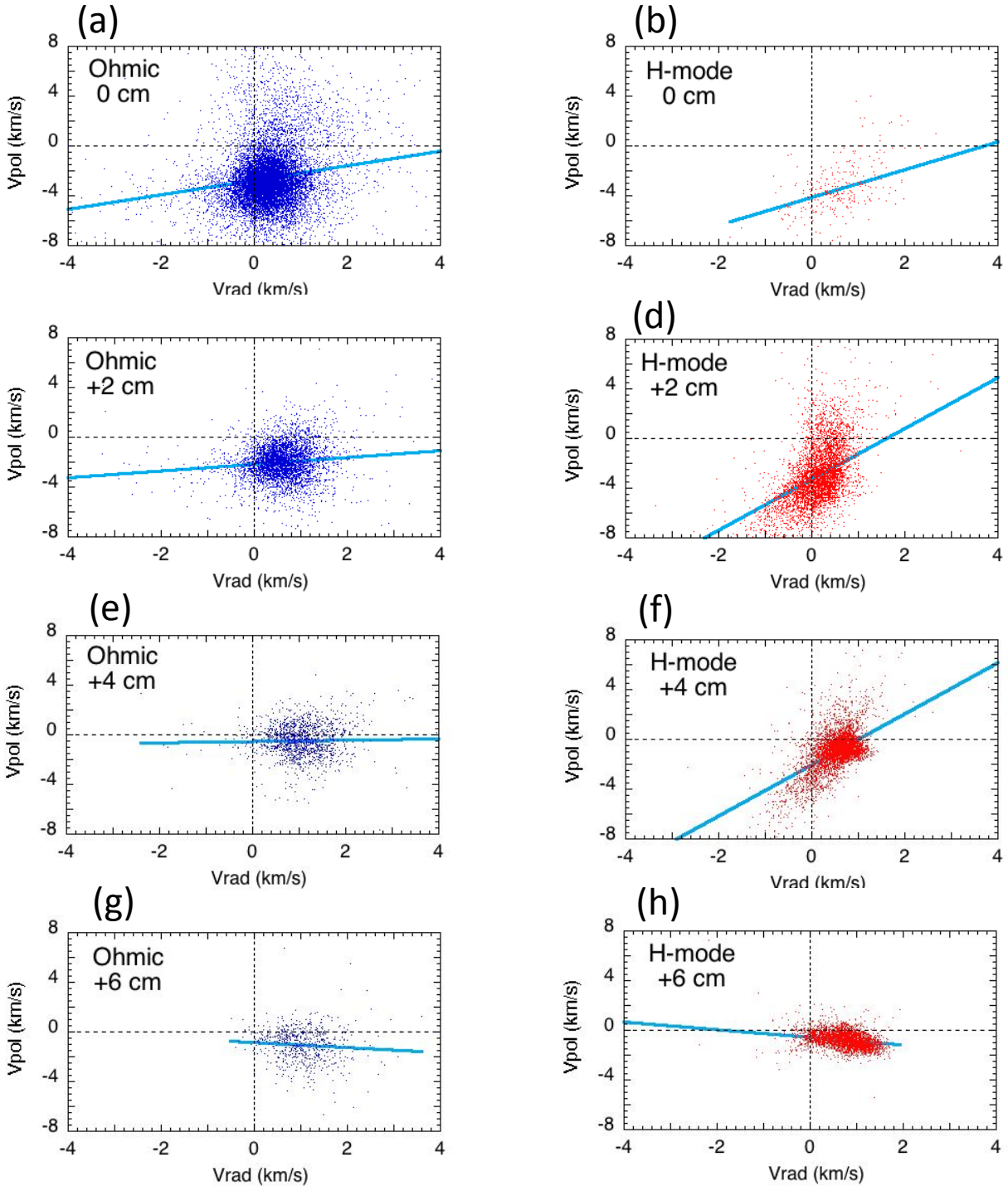
(a)
Ohmic
0 cm
(b)
H-mode
0 cm
Ohmic
+2 cm
(d)
H-mode
+2 cm
(e)
Ohmic
+4 cm
(f)
H-mode
+4 cm
(g)
Ohmic
+6 cm
(h)
H-mode
+6 cm
Vpol (km/s)
Vrad (km/s)

Fig. 11

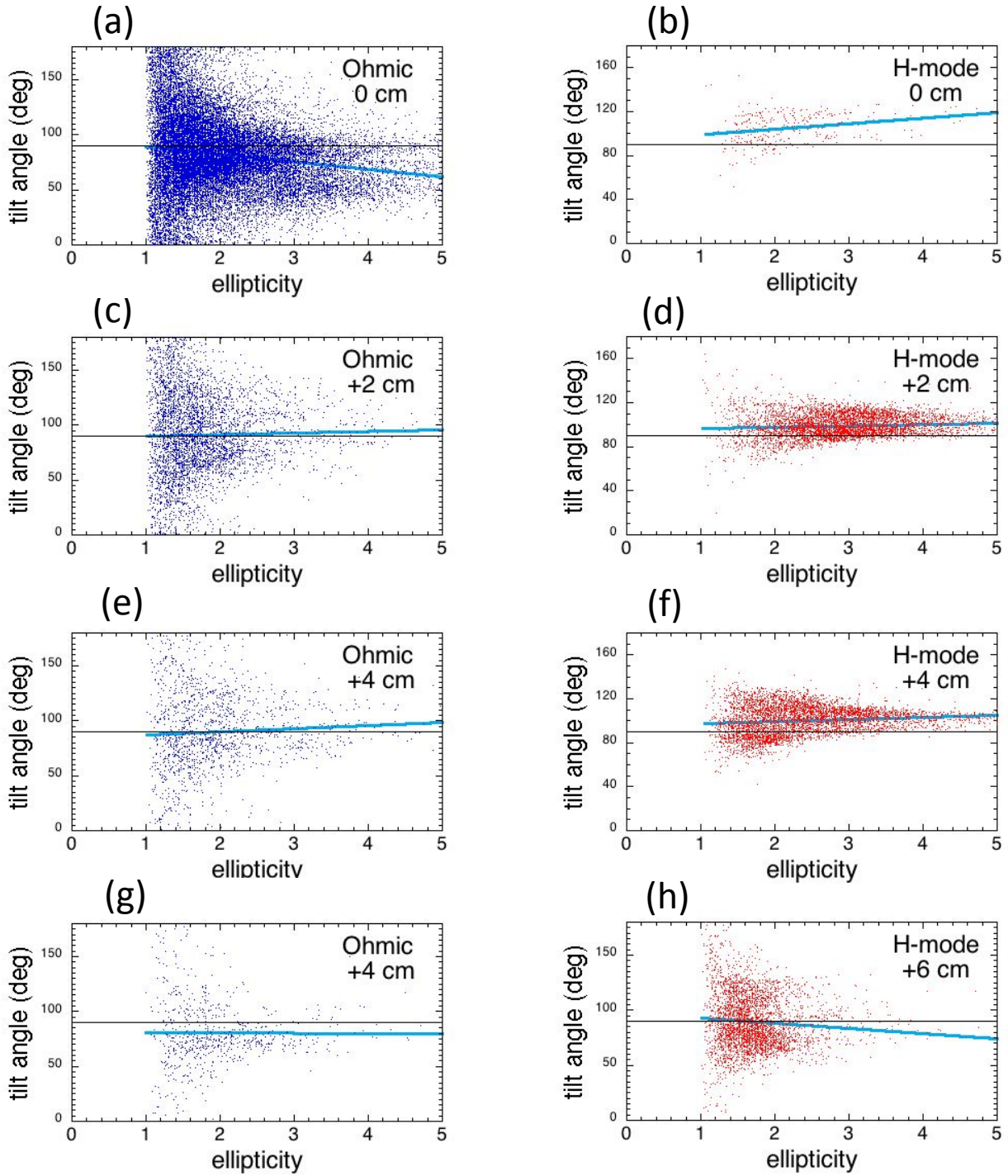
(a)
Ohmic
0 cm
(b)
H-mode
0 cm
(c)
Ohmic
+2 cm
(d)
H-mode
+2 cm
(e)
Ohmic
+4 cm
(f)
H-mode
+4 cm
(g)
Ohmic
+4 cm
(h)
H-mode
+6 cm
tilt angle (deg)
ellipticity

Fig. 12

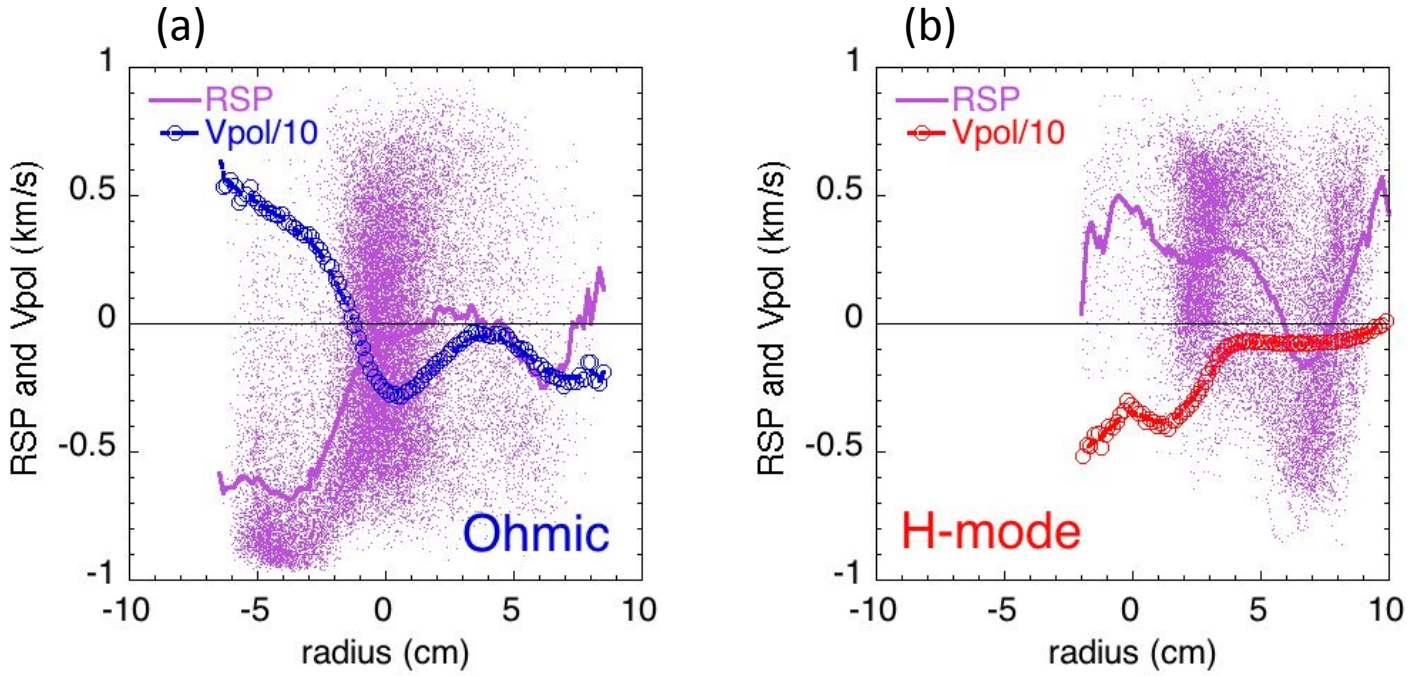
(a)
RSP
Vpol/10
Ohmic
RSP and Vpol (km/s)
radius (cm)
1
0.5
0
-0.5
-1
-10
-5
0
5
10
(b)
RSP
Vpol/10
H-mode
RSP and Vpol (km/s)
radius (cm)

Fig. 13

PPPL PRINCETON PLASMA PHYSICS LABORATORY

Princeton Plasma Physics Laboratory
Office of Reports and Publications

Managed by
Princeton University

under contract with the
U.S. Department of Energy
(DE-AC02-09CH11466)

P.O. Box 451, Princeton, NJ 08543
Phone: 609-243-2245
Fax: 609-243-2751

E-mail: publications@pppl.gov

Website: http://www.pppl.gov